DEPARTMENT OF PHYSICS
UNIVERSITY OF JYVÄSKYLÄ
RESEARCH REPORT No. 8/2015

VUV-DIAGNOSTICS OF LOW TEMPERATURE HYDROGEN PLASMAS

BY
JANI KOMPPULA

Academic Dissertation
for the Degree of
Doctor of Philosophy

To be presented, by permission of the
Faculty of Mathematics and Natural Sciences
of the University of Jyväskylä,
for public examination in Auditorium FYS1 of the
University of Jyväskylä on November 27th, 2015
at 12 o'clock noon

Jyväskylä, Finland
November 2015

PREFACE

The work presented in this thesis has been carried out at the accelerator laboratory of the Department of Physics, University of Jyväskylä during the years 2010–2015.

Foremost, I want to sincerely thank my supervisor Dr. Olli Tarvainen for innumerable discussions, all the support and constant enthusiasm. This thesis was a journey into unfamiliar terrain as there was no earlier experience from emission spectroscopy in the group and I had no earlier experience from plasmas, either. There were rocky hills, dangerous pitfalls and trudging in the darkness during the journey. Nonetheless, at the end of the journey, I also feel that taking a step towards the unknown was a good way to find new paths and interesting questions.

Although the relevant research questions were found early, there were times when I felt that the majority of my time was consumed by preparation and development of diagnostics for countless measurements. However, I would like to thank for those unique opportunities to learn plasma technology, diagnostics, physics and ion sources outside of the core topic of the thesis as well as collaborate with the people around Europe. Special thanks to Dr. Jacques Lettry, Dr. Dan Faircloth, Prof. Daniel Cortázar and their PhD students for offering the possibility to visit their laboratories.

I would like to thank Dr. Taneli Kalvas for all the help and teaching me necessary experimental skills at early stages of the journey. Big thanks also for the entire personnel of the accelerator laboratory. The experiments were mainly performed without dedicated funding by borrowing stuff around the lab and building equipment from scratch with the support and advices given by the technical staff. Special thanks for Dr. Pasi Myllyperkiö at the Department of Chemistry, who kindly borrowed one of the key components of my work, the VUV monochromator.

I want to thank Dr. Hannu Koivisto for the possibility of working in the ion source group and Prof. Rauno Julin for offering me the opportunity for PhD studies. I would like to thank Prof. Motoi Wada and Dr. Robert Welton for reviewing my thesis. I also want thank all the past and current group members, especially Mr. Risto Kronholm, Mr. Janne Laulainen and Dr. Ville Toivanen for enjoyable time and collaboration.

I would like to thank all my friends for the unforgettable moments and spare time activities. I have had the privilege to be a part of those close communities of friends which have developed during the high school and during the studies at the university. Finally, I want to thank my parents all the encouragement and support.

Jyväskylä, November 2015,
Jani Komppula

ACKNOWLEDGEMENTS

This work was supported by the Academy of Finland under the Finnish Centre of Excellence Programme (Nuclear and Accelerator Based Physics Research at JYFL), the EU 7th framework programme 'Integrating Activities – Transnational Access', project number: 262010 (ENSAR) and National Graduate School in Particle and Nuclear Physics.

ABSTRACT

Komppula, Jani
VUV-diagnostics of low temperature hydrogen plasmas
Jyväskylä: University of Jyväskylä, 2015, 61 p.(+included articles)
Department of Physics Research Report No. 8/2015
ISSN 0075-465X; 8/2015
ISBN 978-951-39-6322-4 (nid.)
ISBN 978-951-39-6323-1 (PDF)
Diss.

Vacuum ultraviolet (VUV) emission of low temperature plasmas is rarely studied although it is directly connected to plasma heating and most significant electron impact processes. This thesis describes a theoretical framework for plasma heating power dissipation, presents a robust method to measure VUV-emission and introduces a novel diagnostics for electron impact processes based on VUV emission.

Plasma heating power transformation to light emission, chemical potential and kinetic energy in hydrogen discharges is calculated. The diagnostics of VUV-emission and volumetric electron impact rates, i.e. molecule ionization, dissociation and production of high vibrational levels and metastable electronic states, are applied for filament arc and microwave hydrogen discharges. Those discharges are the most commonly used plasma sources for the production of H^- and H^+ ions, respectively.

The results imply that at least 10% of the plasma heating power is dissipated via photon emission in efficient hydrogen discharges. The measurements imply that the energy efficiency is significantly higher in the filament arc discharge than in the microwave discharge. The comparison of electron impact rates yields information about effects of mechanical solutions on the plasma properties. This information can be used for making predictions and optimization of H^- and H^+ ion sources.

Keywords: Low temperature hydrogen plasma, vacuum ultraviolet emission spectroscopy, plasma diagnostics, ion source

Author

Jani Komppula
Department of Physics
University of Jyväskylä
Finland

Supervisor

Dr. Olli Tarvainen
Department of Physics
University of Jyväskylä
Finland

Reviewers

Prof. Motoi Wada
Graduate School of Science and Engineering
Doshisha University
Japan

Dr. Robert Welton
Spallation Neutron Source
Oak Ridge National Laboratory
USA

Opponent

Dr. Roy McAdams
Tokamak and Neutral Beam Operations Department
Culham Centre for Fusion Energy
United Kingdom

LIST OF INCLUDED ARTICLES

PI J. Komppula and O. Tarvainen. Plasma heating power dissipation in low temperature hydrogen plasmas. *Physics of Plasmas* **22**, *103516 (2015)*.

PII J. Komppula, O. Tarvainen, T. Kalvas, H. Koivisto, R. Kronholm, J. Laulainen and P. Myllyperkiö. VUV irradiance measurement of a 2.45 GHz microwave-driven hydrogen discharge. *Journal of Physics D: Applied Physics*, ***48***, *365201 (2015)*.

PIII J. Komppula and O. Tarvainen. VUV diagnostics of electron impact processes in low temperature molecular hydrogen plasma. *Plasma Sources Science and Technology*, ***24***, *045008 (2015)*.

PIV J. Komppula, O. Tarvainen, S. Lätti, T. Kalvas, H. Koivisto, V. Toivanen and P. Myllyperkiö. VUV-diagnostics of a filament-driven arc discharge H- ion source. *AIP Conference Proceedings*, ***1515***, *66 (2013)*.

The author has performed most of the experimental and theoretical work, the data analysis and numerical calculations in all of the publications. The publications listed above are included in the appendixes of the thesis.

CONTENTS

1 INTRODUCTION

Motivation for this thesis arose from a simple question: "How much vacuum ultraviolet (VUV) radiation is emitted by low temperature hydrogen plasmas?" Since some of the first steps of plasma physics were taken with glow discharges [1] and hydrogen plasmas have been studied intensively over half a century [2–4], this question was supposed to be almost trivial. But it was not.

The origin of the question was related to technical development of negative hydrogen ion sources. These ion sources play a crucial role in particle accelerators and magnetic confinement fusion research [5]. The use of H^- ions allows charge exchange injection into circular proton accelerators or storage rings, such as LHC (CERN) and SNS (ORNL). Also smaller particle accelerators, (e.g. K130, MCC30/15 and Pelletron at JYFL), use H^-. This is because negative hydrogen ions allow more efficient ion beam extraction from the cyclotrons (K130, MCC30/15) in comparison to protons or because the operating principle of the accelerator requires using negative ions (Pelletron). Magnetic confinement fusion research requires energetic beams of neutral hydrogen/deuterium atoms for heating the plasma in tokamaks up to the burning temperature. The most efficient way to produce them in the energy range required by recent and future experiments (e.g. LHD and ITER) is from H^-/D^- beams by stripping the additional electron.

Negative hydrogen ions are produced with low temperature plasmas by two different processes [5]. The surface production occurs due to the interaction between hydrogen plasma and low work function surface facing the plasma. In the plasma volume, negative hydrogen ions are formed by dissociative attachment (DA) of electrons to ro-vibrationally excited hydrogen molecules.

The negative hydrogen ion sources can be optimized for surface or volume production, but the highest performance ion sources utilize both production mechanisms [5]. Thin layer of caesium is used for lowering the work function of the surfaces and subsequently increase production of negative ions. The volume production can be optimized by enhancing densities of low energy electrons and hydrogen molecules at high ro-vibrational levels.

Thin layer of caesium is typically formed by seeding caesium into the plasma.

Controlling of the caesium coverage is difficult, because the caesium affects the plasma dynamics and its adsorption / evaporation rate is sensitive to surface temperatures of the plasma source. Furthermore, caesium is a highly reactive element. Thus, a suitable replacement for caesium has been searched, but has not been found so far. One of the replacements could be diamond [6]. Exposure of hydrogen-terminated diamond surface to UV-light excites electrons to the conduction band, which lies above the vacuum level [7]. These electrons have negative electron affinity (i.e. work function) and they can efficiently produce negative hydrogen ions on the surface [8]. However, necessary information about VUV-emission of low temperature plasmas was not available, which was the original motivation for this thesis.

From the theoretical point of view, a theoretical framework which could be used for estimating the VUV-emission of low temperature plasmas was not found. Also numerical simulations are rarely found from the literature [9]. Therefore, such framework for heating power dissipation in low temperature plasmas was developed and applied for hydrogen plasmas.

Generally utilized measurement methods of the absolute VUV-emission are challenging to apply to plasma sources [10, 11]. This is because the calibration of the spectrometers is sensitive to the measurement geometry and VUV optics are temporally unstable in typical vacuum conditions of plasma sources. Development of a robust and straightforward method to measure absolute VUV-emission from hydrogen plasma sources was required for this thesis.

VUV-emission itself provides information about plasma processes in low temperature plasmas. The main dissociation channels of hydrogen molecules are directly related to VUV-emission, as well as the main production channel of high vibrational levels. Furthermore, the ionization rate is proportional to electronic excitations (VUV-emission) almost independently of the plasma parameters, e.g. electron temperature. Hence, a diagnostics method for the most significant electron impact processes in low temperature hydrogen plasmas was developed.

The information about the VUV-emission and plasma processes provided by this thesis was challenging to obtain with methods introduced earlier. It was also found that plasma sources are highly sensitive to mechanical design and operational procedures. Therefore, this thesis focuses on the methods instead of the results given by them. The most reliable and generalizable results were achieved with a filament driven arc multicusp discharge, LIISA [PIII, PIV].

The introduced methods can be directly applied to development of H^+, H_2^+ and H^- ion sources. This is because the plasma processes, for which the diagnostics is developed, are directly connected to production of hydrogen ions. Because measurements and analysis can be performed straightforwardly, mechanical modifications can be connected to changes of the plasma process rates. Furthermore, the thesis provides better understanding about plasma heating power dissipation. This is necessary for ion source development, because the maximum level of the injected heating power is limited by technical choices

It is worth noting that information about VUV-emission and plasma processes of low temperature plasmas are rarely available in the literature at general

level. Low temperature plasmas are widely applied [12], for example, in material processing [13–16], gas decomposition [17, 18], biomedical applications [19] and plasma thrusters [20]. Furthermore, similar types of low temperature hydrogen plasmas are found from the edge of thermonuclear fusion machines [21] and interstellar space [22]. Although this thesis focuses on the plasmas of the hydrogen ion sources, the methods and reasoning can be applied to a wide range of plasmas.

The thesis is outlined as follows. Chapter 2 presents physical background required for the understanding of the work. The main scientific work is presented in chapters 3, 4 and 5. The theoretical framework for plasma heating power dissipation is described in chapter 3, the developed apparatus for VUV-emission measurements is presented in chapter 4 and chapter 5 explains VUV-diagnostics of plasma processes. The methods were applied to a filament driven multicusp arc discharge and a 2.45 GHz microwave discharge. These results are presented in chapter 6.

2 BACKGROUND

2.1 Hydrogen atom and molecule

This thesis focuses on the emission spectroscopy of low temperature hydrogen plasmas. In order to understand the origin of the light emission it is necessary to study the properties of the hydrogen atom and molecule at the quantum level. This section explains briefly the principles of atomic and molecular spectroscopy.

The hydrogen atom and molecule are the simplest atom and molecule in the universe. The hydrogen atom consists of a proton and an electron, which are attracted by the electromagnetic force. The hydrogen molecule is produced by two hydrogen atoms bound together. Both the hydrogen atom and molecule are electrically neutral particles.

A quantum mechanical system, such as the hydrogen atom or molecule, can be described with the Schrödinger equation. The Schrödinger equation cannot be subjected to firm proof but was put forward as a postulate, based on the analogy between the wave nature of light and the electron [23]. Any quantum mechanical system can be accurately described with the Schrödinger equation, but there are challenges to solve it accurately for more complex systems than the hydrogen atom. This thesis does not focus on the methods of solving the Schrödinger equation, but uses solutions as properties of the hydrogen atom and molecule. However, the plasma diagnostics and the plasma dynamics presented in this thesis are deeply connected to the properties of the Schrödinger equation (solutions) of the hydrogen atom and molecule as explained later.

The hydrogen atom and molecule can be treated as an electron(s) orbiting a stationary proton(s) due to great velocity and mass differences between the electron and the proton. From this thesis point-of-view, the most important properties of the hydrogen atom and molecule can be described with the time independent Schrödinger equation for the electron

$$-\frac{\hbar^2}{2m}\nabla^2\psi(\boldsymbol{r}) + V\psi(\boldsymbol{r}) = E\psi(\boldsymbol{r}) \tag{2.1}$$

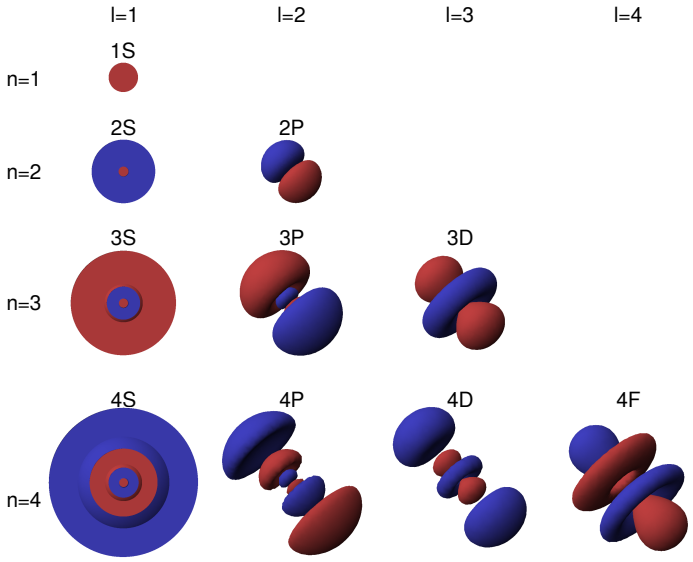

FIGURE 1 Lowest orbitals of the hydrogen atom. Orbitals have been categorized with main quantum number (n) and angular momentum quantum number l. Notation of the state is presented over the orbital ($1S$, $2S$, $2P$, etc.) The orbitals are produced with Orbital Viewer [24].

where $\hbar$ is the reduced Planck constant, m is the mass of the electron, ∇^2 is the Laplace operator, V is the electric potential, ψ is the wave function of the state and E is the energy of the state. Typically, the potential well V caused by the proton(s) is known or can be estimated, while multiple different discrete states (ψ, E pairs) are found as solutions of the equation. The lowest energy state is denoted as the ground state, while higher energy states are called excited states.

2.1.1 Structure of the hydrogen atom

The wave function describes the probability of finding the electron at a particular position. The more practical way to indicate the most probable position of the electron is to use the term orbital. The orbital describes the volume from where the electron can be found with a 95% probability. The lowest orbitals of the hydrogen atom are presented in Fig. 1. The shapes and symmetries of the atom orbitals are categorized with the quantum numbers n, l and m, which are useful in understanding of the electron transitions between the states. The main quantum number n describes the total energy of the state, l describes the angular momentum of the state and m describes the angular momentum vector component. This thesis uses notation nl, where the main quantum number n is represented by natural numbers (1, 2, 3, etc) and the angular momentum quantum number l is represented with letters (S, P, D and F). Thus, the lowest states of the hydrogen atom are $1S$, $2S$, $2P$, $3S$, $3P$, $3D$, etc.

The electron can only transfer from one state to another or it can be removed from the potential well of the nucleus (ionization). In a separated atom or molecule these transitions can occur only by absorbing or emitting a quan-

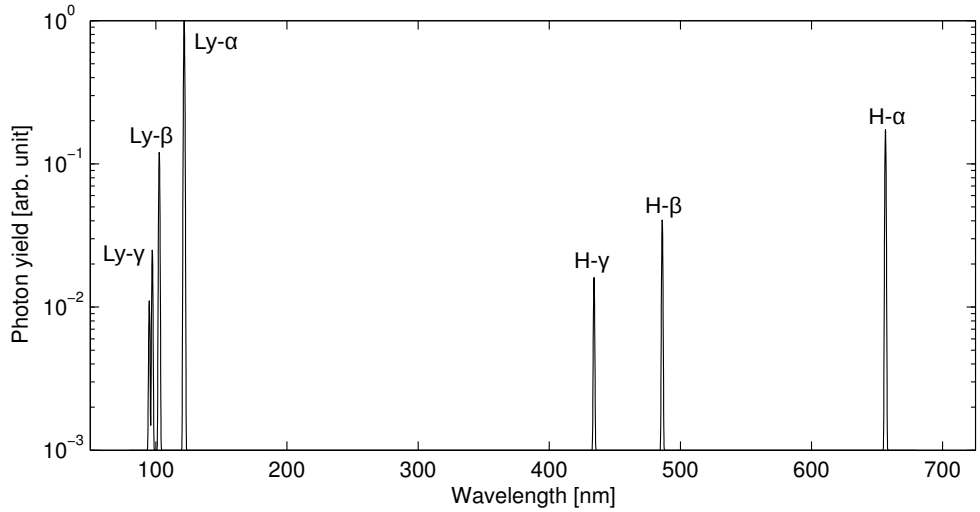

FIGURE 2 Synthetic spectrum of the hydrogen atom ($n \leq 5$) excited by electron population with T_e=6.5 eV. Calculated using cross sections from Ref. [25] and transition probabilities from Ref. [26].

tum of light, photon, whose energy corresponds to the energy difference of the states. The transition energy can be also carried by impacting particle, e.g. electrons. Transitions from upper states to lower states produce a discrete light spectrum (Fig. 2). The transitions are referred based on the main quantum number of the lower state. For example, Lyman-series in the VUV range corresponds to transitions from excited states to ground state, e.g. Ly−α (H(n=2)→H(n=1)), Ly−β (H(n=3)→H(n=1)), etc, and Balmer-series in visible light range corresponds to transitions to n=2 state, e.g. H−α (H(n=3)→H(n=2)), H−β (H(n=4)→H(n=2)), etc.

The transition probability between states, $A_{a\to b}$, is proportional to the wave functions and the transition moment, i.e.

$$A_{a\to b} \propto \int \psi_a^*(\boldsymbol{r})\, \boldsymbol{\mu}\, \psi_b(\boldsymbol{r})\, d^3\boldsymbol{r}, \tag{2.2}$$

where ψ_a^* is the complex conjugate of the wave function of the state a, $\boldsymbol{\mu}$ is the transition moment operator and ψ_b is the wave function of the state b. Transitions between electron orbitals and molecule vibrational levels are described mainly by the electric dipole moment. The electric dipole moment depends only on the positions and the charges of the particles, e.g. for hydrogen atom

$$\boldsymbol{\mu} = q\,\boldsymbol{r}, \tag{2.3}$$

where q is the chrage of electron and $\boldsymbol{r}$ is the position.

The transitions are classified allowed and forbidden based on the transition probability. The transition is allowed, if the transition probability is non-zero i.e. the symmetries of the wave functions ψ_a and ψ_b are different. Because the symmetry of the wave function is described by the quantum numbers (e.g. n, l and m for atom), the allowed transitions can be concluded from the quantum numbers. These conclusions, namely the selection rules for atoms are:

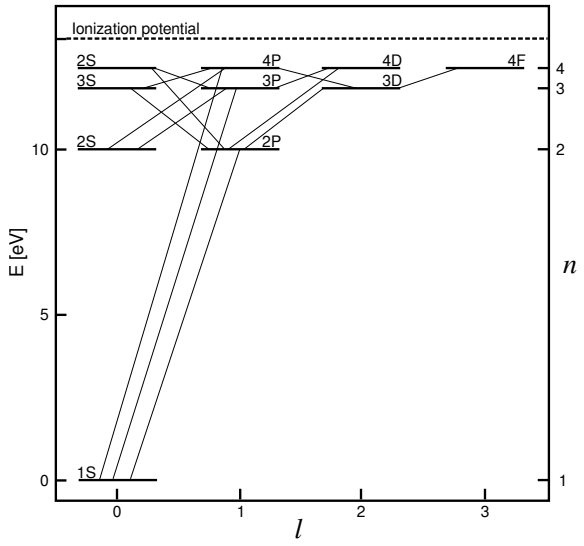

FIGURE 3 Optically allowed transitions between lowest electronic states of the hydrogen atom for excited states $n \leq 4$. Transition probabilities and energy levels are from Ref. [26].

1. Δn is unrestricted
2. $\Delta l = \pm 1$

Excited states decay spontaneously to the lowest possible state by emitting photons. Lifetimes of excited states are determined by the transition probabilities to lower states. The majority of excited states decay to the ground state within nanoseconds [26, 27]. However, there are excited states which can not decay to the ground state via allowed transitions. These metastable states have orders of magnitude longer lifetimes than regular excited states. For example, the hydrogen atom has one metastable state $2S$, whose lifetime is on the order of milliseconds [28]. A summary of excited states and allowed transitions of the hydrogen atom is presented in Fig. 3.

2.1.2 Structure of the hydrogen molecule

The structure of the hydrogen molecule is more complex than the structure of the hydrogen atom due to orbital interactions between the atoms, the electron spin and rotational-vibrational motion of the molecule. In principle, orbitals, rotational-vibrational levels and transition probabilities are calculated identically to the hydrogen atom, i.e. by solving the Schrödinger equation and calculating the transition probabilities from the wave functions and the transition moment. Detailed technical descriptions of the calculations can be found from the literature [23, 29].

The hydrogen molecule has three different types of quantum states. Electronic states describe orbitals of the electrons while vibrational and rotational levels describe vibrational and rotational motions of the molecule. From the point-of-view of this thesis the structure of the hydrogen molecule can be described

with electronic states and vibrational levels. Rotational levels are not taken into account because they have a negligible effect to electronic excitations due to minimal energy exchange (≈0.01 eV) in transitions and long collision times ("frozen rotation") [25].

A quantum mechanical property of particles, *spin*, affects the orbitals and transitions if the system consists of more than one identical particle. Electrons are fermions, i.e. they have half-integer spin which points up or down[1]. The Pauli exclusion principle dictates that two identical fermions cannot occupy the same quantum state simultaneously. Thus, only two electrons which have opposite spins can be at the same state, for example at the ground state of the hydrogen molecule.

Electronic states of the hydrogen molecule can be described with five different quantum numbers by using the notation

$$N^{2S+1}\Lambda_{\sigma}^{\pi},$$

where N denotes the united atom principal quantum number (X, B, C, D, ...), S is the total electronic spin, Λ is the total angular momentum quantum number (Σ, Π, Δ, ...), σ is the label of its g/u symmetry and π is the parity of the state (+/-) [29]. Allowed transitions between electronic states are governed by the following selection rules:

1. $g \leftrightarrow u$
2. $\Delta S = 0$
3. $\Delta\Lambda = 0, \pm 1$

The Pauli exclusion principle does not restrict the spin direction of the electron on the excited states. However, the spin direction can not be changed during the transitions between electronic states. Therefore, transitions between states which have different spins are strongly forbidden. The excited states are called singlet and triplet states depending on the direction of the electron spin with respect to the ground state. Singlet states have an opposite spin than the ground state, while triplet states have a parallel spin to the ground state. Thus, the hydrogen molecule has two strongly separated multiplet systems of electronic states which differ by the orientation of the electron spins. Only singlet states are allowed to decay to the ground state $X^1\Sigma_g^+$. The lowest triplet state, $b^3\Sigma_u^+$, to which virtually all triplet excitations decay, is repulsive and it results to molecule dissociation. The hydrogen molecule has also a metastable triplet state, $c^3\Pi_u$. The electronic states and allowed transitions of the hydrogen molecule are presented in Fig. 4.

Each electronic state has its own structure of vibrational levels (see Fig. 4b). Vibrational levels of a diatomic homonuclear molecule, such as H_2, are metastable [23]. Thus, vibrational excitations do not decay spontaneously, but change in collisions with other molecules [31], walls of the plasma chamber (e.g. Refs. [32–34] and references therein) and due to vibronic (electronic) excitations [35].

[1] In this context up and down do not refer to physical directions but are indicators of spin directions at an abstract level.

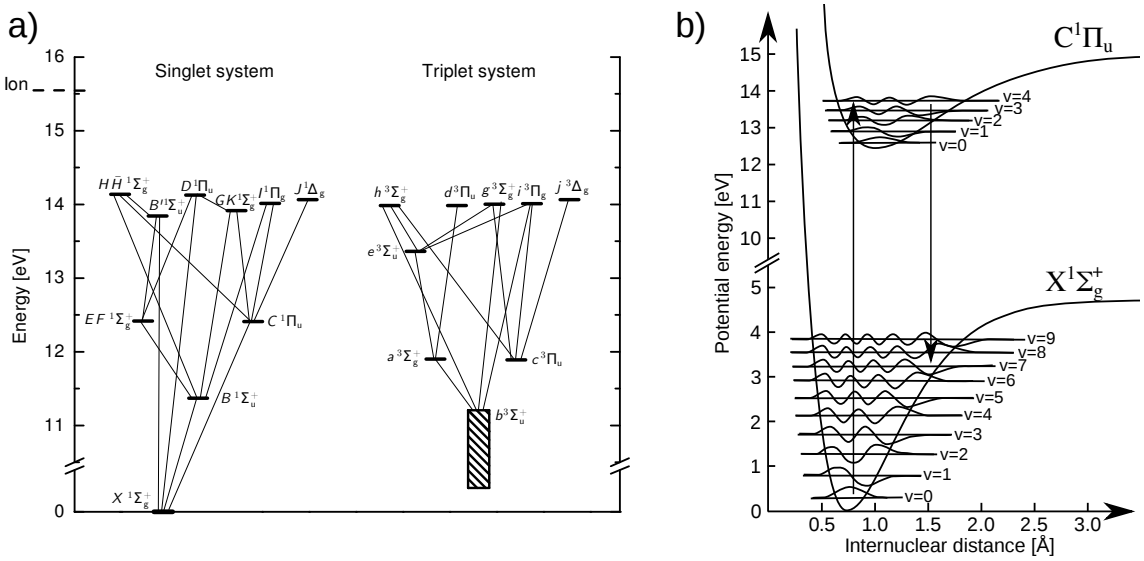

FIGURE 4 **(a)** Optically allowed transitions between lowest excited states of the hydrogen molecule. **(b)** Schematic picture of Franck-Condon principle during the $X^1\Sigma_g^+ \rightarrow C^1\Pi_u$ excitation. Data is from Ref. [30].

A simultaneous change of the electronic state and the vibrational level of the molecule is called vibronic transition. Vibronic transition probabilities are governed by the Franck–Condon principle [30]. The Franck–Condon principle assumes that the vibrational motion of the molecule is slow in comparison to the time scale of electronic transition (e.g. photon emission). Therefore, the transition probabilities of vibronic transitions can be divided into transition probabilities of the electronic states and those of the vibrational levels. The transition probabilities of vibrational transitions are called Franck-Condon factors.

Due to the Franck-Condon principle electronic (vibronic) transitions of hydrogen molecules produce emission bands instead of discrete lines. Each line of the emission band corresponds to individual transition from one vibrational level on the upper electronic state to another vibrational level on the lower electronic state. The lowest singlet transitions, $B^1\Sigma_u^+ \rightarrow X^1\Sigma_g^+$ and $C^1\Pi_u \rightarrow X^1\Sigma_g^+$, of the hydrogen molecule are in the VUV-range and are called Lyman- and Werner bands, respectively. The lowest triplet transitions ($a^3\Sigma_g^+ \rightarrow b^3\Sigma_u^+$) produces continuous spectrum, because the $b^3\Sigma_u^+$ state is repulsive. Thus, the lowest triplet transition $a^3\Sigma_g^+ \rightarrow b^3\Sigma_u^+$ is called molecular continuum. A synthetic emission spectrum of the hydrogen molecule is presented in Fig. 5.

2.1.3 Electron impact excitations

In low temperature plasmas atoms and molecules are typically excited by electron impact, while excitations decay via spontaneous emission. The probability of electron impact excitation can be described with the cross section σ, which illustrates an effective cross sectional area of the atom or molecule. Only electrons whose energy exceeds the excitation (threshold) energy can excite atoms or

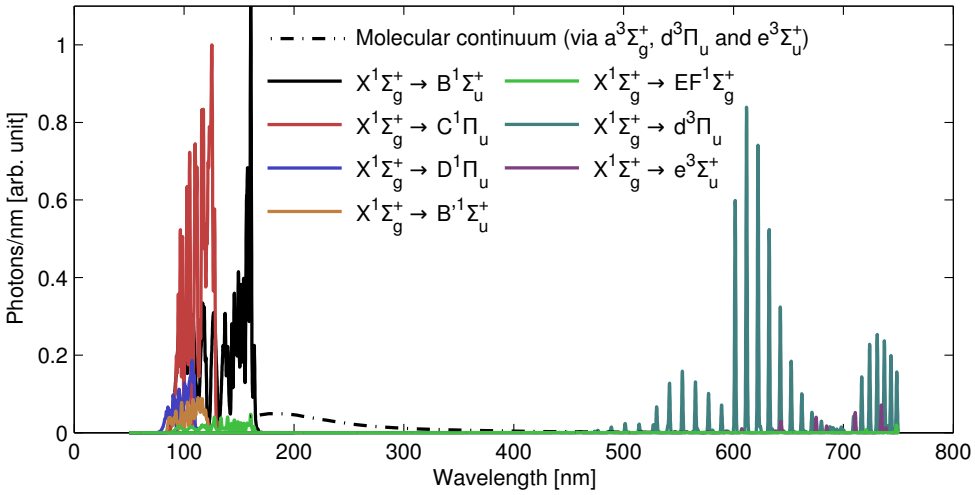

FIGURE 5 A synthetic spectrum of the hydrogen molecule produced by the most significant electron impact excitations (T_e=6.5 eV). Different colours indicate different excitation channels excluding the molecular continuum corresponding to the total emission caused by all triplet excitations. Calculated using cross sections from Ref. [25] and transition probabilities from Ref. [30].

molecules. The cross section depends on the transition and electron energy. The functional shapes of the electron impact excitation cross sections are determined by the type of the transition (selection rules) [36].

In the case of hydrogen atom excitations occur via coulomb excitations, i.e. through the electromagnetic field generated by the projectile electron. Cross sections for optically (dipole) allowed excitations have broad energy dependences that typically reach a peak value at energies equal to about four times the threshold energy, and have a slow decline at higher energies (see Fig. 7 in section 2.3). Cross sections of dipole-forbidden excitations, e.g. from the ground state 1S to 2S or 3S states, typically have narrow peaks with a maximum within two to three times the threshold energy [36].

Excitations to singlet states are spin allowed in the case of hydrogen molecule and, therefore, their excitation cross-sections depend on selection rules similarly to those of the hydrogen atom. This means that the cross sections of most singlet excitations are broad due to optically (dipole) allowed nature of the transitions (see Fig. 8a in section 2.3). The cross section of $X^1\Sigma_g^+ \rightarrow EF^1\Sigma_g$ singlet excitation is dipole forbidden and is therefore peaked at lower electron energies.

Spin-forbidden excitations occur due to electron exchange processes. This means that the incident electron is captured by the molecule into an excited state while the other electron of the molecule with the opposite spin is ejected [36]. Thus, the cross sections of (spin forbidden) excitations to triplet states reach a maximum very close to the threshold, and decrease rapidly at higher electron energies (see Fig. 8a in section 2.3).

A general rule of thumb, based on the quantum numbers, for magnitudes of the cross sections can not be found from the literature. The cross section mag-

nitudes are affected by the radial wave function overlap of the initial and final states [36]. For example, by studying the electron impact excitation cross sections of the hydrogen atom [25], it can be argued that the lowest excited states ($n \leq 4$) cover the majority (>90%) of the total excitation cross section. The given excitations emit more than 80% of the photons in the VUV range (<200 nm). Vibrational level of the ground state in the hydrogen molecule affect both, the threshold energies and magnitudes of the cross sections. Increasing vibrational level lowers the threshold energies of the processes. The magnitude of excitation cross sections of optically allowed transitions depend on vibrational level up to a factor of three.

The effect of the metastable states in low temperature plasmas where the average electron energy is lower than the ionization energy can be similar to another neutral species. Metastable states lie significantly above the ground state and, therefore, ionization potentials of the metastable states are lower than ionization potentials of ground states. Thus, a significantly larger fraction of the electron population can ionize metastable atoms or molecules. However, the dynamics of the metastable atoms and molecules are complex. They are sensitive to electron impact de-excitation and collisional quenching as well as interaction with the walls of the plasma chamber (e.g. see Refs. [37, 38] and references therein).

Electron impact cross sections of the hydrogen atom are well known, but there are still uncertainties related to the electron impact cross sections of hydrogen molecule and structure of the $c^3\Pi_u$ triplet state. Most of the cross section data are only available for a limited number of excited states and the lowest vibrational level of the ground states, $X^1\Sigma_g^+(v{=}0)$ [25]. Moreover, there is a lack of experimental validation of the cross section data especially close to the threshold energies [39, 40], which is the most relevant range for low temperature plasmas. The lifetime of the $c^3\Pi_u$ state depends significantly on the vibrational level and the parity of the state ($c^3\Pi_u^-$ and $c^3\Pi_u^+$). The $c^3\Pi_u^-$ state is metastable with the radiative lifetime varying from 1 ms (v=0) to 10 μs (v=3) [27, 41]. There are only few studies on the $c^3\Pi_u^+$ state, with significant discrepancy between calculations and experiments [27]. In the electron impact cross section data the $c^3\Pi_u$ state is argued to be metastable without any distinction between the parities of the wave function [25]. Moreover, experimental and theoretical values of the electron impact excitation cross sections differ by a factor of 2–3 [25, 42]. Because there are no cross section data on electron impact excitation to the $c^3\Pi_u^+$ state, the $c^3\Pi_u$ state is assumed to behave as the metastable $c^3\Pi_u^-$ state.

Several reviews about electron impact cross sections in low temperature hydrogen plasmas can be found from the literature (e.g. Refs. [25, 39, 40, 43, 44]). Data from Ref. [25] have been used in this study because they include the most complete critically assessed set of cross sections including fitting functions in analytic form. Due to available data singlet states $B^1\Sigma_u^+$, $C^1\Pi_u$, $D^1\Pi_u$, $EF^1\Sigma_g^+$, $B'^1\Sigma_u^+$, $D'^1\Pi_u$ and triplet states $a^3\Sigma_g^+$, $b^3\Sigma_u^+$, $c^3\Pi_u$, $e^3\Sigma_u^+$ and $d^3\Pi_u^+$ are taken into account in this thesis.

2.2 Low temperature plasma

Plasma is one of the four states of matter in addition to solid, liquid and gas. When gas (or at least free electrons) is heated enough a fraction of atoms and/or molecules are ionized. By the definition plasma is formed, when the gas consists of freely moving charged particles with sufficient density to interact collectively[2]. In this state plasma is quasi-neutral and behaves like an electric conductor leading to almost constant electric potential inside the plasma volume.

Dynamics of the plasma result from the collective interactions of charged particles and neutrals. It is affected by both quantum mechanical properties of the particles and electromagnetic fields created by external sources or the particles themselves. Plasma dynamics are governed by fluid dynamics (Navier–Stokes equations), electromagnetism (Maxwell's equations) and non-equilibrium thermodynamics. Applying these fields of physics together the plasma can be described at fundamental level with Vlasov-Maxwell-Boltzmann system of equations. For example, the description of the atomic hydrogen plasma, which is the simplest plasma consisting of electrons (e), ions (i), neutrals (n) and metastable atoms (n^*), requires ten equations

$$\frac{\partial f_e}{\partial t} + \boldsymbol{v}_e \cdot \nabla f_e - \frac{q}{m_e}\left(\boldsymbol{E} + \boldsymbol{v_e} \times \boldsymbol{B}\right) \cdot \nabla_v f_e = Q(f_e, f_i, f_n, f_{n^*}) \tag{2.4}$$

$$\frac{\partial f_i}{\partial t} + \boldsymbol{v}_i \cdot \nabla f_i + \frac{q}{m_i}\left(\boldsymbol{E} + \boldsymbol{v_i} \times \boldsymbol{B}\right) \cdot \nabla_v f_i = Q(f_i, f_e, f_n, f_{n^*}) \tag{2.5}$$

$$\frac{\partial f_n}{\partial t} + \boldsymbol{v}_n \cdot \nabla f_n = Q(f_n, f_e, f_i, f_{n^*}) \tag{2.6}$$

$$\frac{\partial f_{n^*}}{\partial t} + \boldsymbol{v}_{n^*} \cdot \nabla f_{n^*} = Q(f_{n^*}, f_e, f_i, f_n) \tag{2.7}$$

$$\nabla \times \boldsymbol{B} = \mu_0 \boldsymbol{j} + \frac{1}{c^2}\frac{\partial \boldsymbol{E}}{\partial t} \qquad \nabla \times \boldsymbol{E} = -\frac{\partial \boldsymbol{B}}{\partial t} \tag{2.8}$$

$$\nabla \cdot \boldsymbol{B} = 0 \qquad \nabla \cdot \boldsymbol{E} = \frac{1}{\epsilon_0}\rho \tag{2.9}$$

$$\rho = q\int (f_i - f_e) d^3v \qquad \boldsymbol{j} = q\int (f_i \boldsymbol{v}_i - f_e \boldsymbol{v}_e) d^3v \tag{2.10}$$

where q is the elementary charge, m is the mass, $\boldsymbol{E}$ and $\boldsymbol{B}$ represent the collective self-consistent local electromagnetic field, c is the speed of light in vacuum, ρ is the charge density, $\boldsymbol{j}$ is the electric current density and $\boldsymbol{v}$ is the velocity. The distribution function f_α of the species α depend on the location $\boldsymbol{r}$, velocity $\boldsymbol{v}$ and time t. The mathematical operator $Q(f_\alpha, f_{\beta_1}, f_{\beta_2}, f_{\beta_3})$ describes changes in the distribution function f_α caused by elastic and inelastic collisions with species β_1, β_2 and β_3.

[2] This condition can be defined formally with the parameter *Debye length*. Debye length is the characteristic length scale which mobile charge carriers (e.g. electrons) screen out electric fields. By definition, Debye length in the plasma must be significantly shorter than the physical dimensions of the plasma.

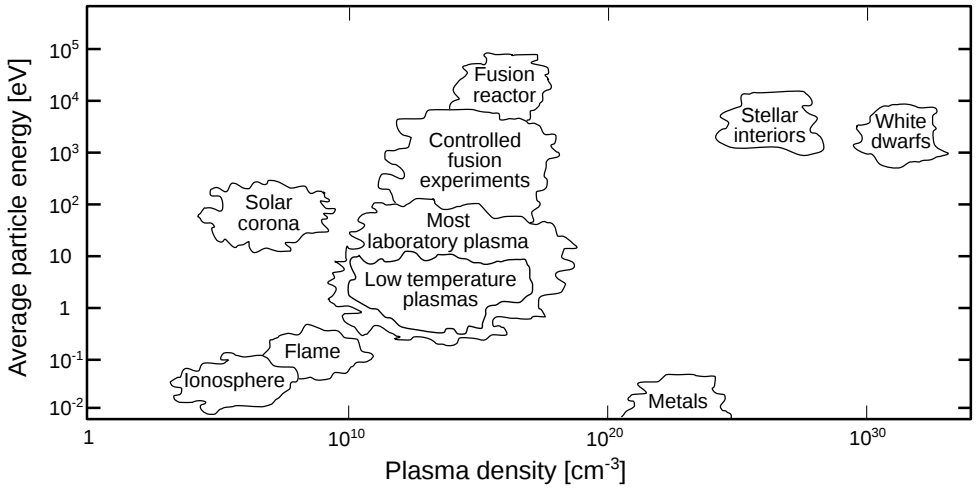

FIGURE 6 Ranges of space and laboratory plasmas as a function of plasma density and average particle energy. Data is from Ref. [46].

Equations 2.4–2.7 describe the particle dynamics in the plasma. The left hand sides of the equations describe the collective dynamics and motions of the particles in electromagnetic fields while the right hand sides of the equations describe discrete collisions between particles. Equations on 2.8 and 2.9 are Maxwell's equations. They set boundary conditions for the electromagnetic fields and describe how charged particles themselves affect the electromagnetic fields. Equations 2.10 describe relations of the distribution functions and velocity to the charge density and the electric current density. This system of equations is impossible to solve directly[3]. Also numerical simulations require several assumptions which are valid only within a limited range of plasma parameters

Plasmas are typically classified with the plasma (electron) density and temperature (Fig. 6). This thesis focuses on low temperature plasmas where the lowest excited states of the neutral particles are in corona equilibrium. Such hydrogen plasmas have the following properties, which virtually all hydrogen ion sources fulfill:

- The plasma is not in thermal equilibrium
- The plasma density n_e is below 10^{16} cm^{-3}
- The ion temperature T_i is lower than the electron temperature T_e
- The neutral gas pressure is under 500 Pa
- The ionization degree is low, i.e. $\frac{n_e}{n_n+n_e} \ll 1$

Low temperature plasmas are not in thermal equilibrium, which means that the average energies of neutral particles, ions and electrons differ significantly [13].

[3] *Impossible* is a strong argument in science but it is probably justified in this context. This is because the system of equations consists of multiple partial differential equations, which are challenging to solve even separately. For example, the smoothness and existence of solutions of the Navier-Stoke equations, which are simplified part of the system of equations 2.4–2.7, is one of the Millennium Prize Problems [45].

The average energy of the neutral particles is typically comparable to room temperature air, while the average energies of ions and electrons are typically 30 and 300 times higher, respectively. In fact, it is unnatural to use the expression *temperature*, which refers to Maxwellian or Boltzmann distributions, in low temperature plasmas. This is because the particle distributions differ from the ideal Maxwellian or Boltzmann distributions affecting the plasma dynamics significantly. The formation and functional shapes of particle distributions are explained more precisely in Section 2.4

The corona equilibrium assumes that electronic excitations decay via spontaneous emission. In the corona equilibrium majority of atoms and molecules are on the electronic ground state. The maximum applicable plasma density is limited by the lifetime of the excited states, i.e. the plasma density is required to be low enough to guarantee that electron impact de-excitation from the excited states is negligible. Correspondingly the excitation transfer between neutral particles limits the maximum pressure. The ion temperature is limited by the assumption that excitation and ionization occurs due to electron impact processes. Such conditions are typically achieved at low ionization degree although it is not a strict requirement itself.

Low temperature plasmas are heated by transferring energy to the electrons (see detais in section 2.6). Therefore, hot electrons (E_e>6 eV) are responsible for the most important plasma processes, such as ionization, production of high vibrational states of molecules and dissociation. This thesis focuses on the dynamics of hot electrons.

Accurate modelling of low temperature plasmas does not allow significant simplifications of the Vlasov–Maxwell–Boltzmann system of the equations. Thus, the most sophisticated numerical methods use several models to describe equations 2.4–2.10 [47]. For example, a recent study of the VUV photon fluxes emitted by a low temperature noble gas plasmas uses five different models to describe electromagnetism, electron energy transport, reaction kinetics, fluid kinetics and radiation transport [48]. Particle-in-cell–Monte-Carlo (PIC–MC) simulations [49] and plasma chemistry models [50] are widely used for modelling plasma sources. The PIC-MC simulations are based on particle-in-cell solution for fluid dynamics of the plasma (left hand sides of the equations 2.4–2.7 and equations 2.8 and 2.9) and combine this with Monte-Carlo simulation of impact processes (right hand side of the equations 2.4–2.7). The PIC-MC simulations provide reasonably accurate spatial information about the plasma, but they require a lot of computing time. Plasma chemistry models are typically based on separated, simplified, calculation of the global electron energy distribution in the plasma (Eg. 2.4) which is used for global plasma chemistry calculations (right hand side of the equations 2.4–2.7). However, there is a concern of uncertainties and validation of these models [47,49,50] where the hot electron impact processes have a significant role.

The majority of theoretical and numerical studies of plasmas are focused on the solutions of the Vlasov–Maxwell–Boltzmann system. For this approach, the plasma density and particle distribution functions are key elements to which the majority of plasma diagnostics is focused on [13, 51]. The point-of-view of

this thesis is slightly different. It is based on the following statements about low temperature plasmas:

- the lifetime of the ions and electrons is short, i.e. the plasma density is a balance between ionization and plasma losses
- the first step of plasma heating power dissipation is through inelastic electron impact collisions including ionization and electron excitation of neutrals
- the electron energy distribution can be mathematically described and it can vary spatially, temporally and depend on the mechanical design of the plasma source

Using these statements as a starting point, plasmas can be treated mathematically separately from the Vlasov–Maxwell–Boltzmann system of equations by studying the probabilities of electron impact processes. However, this approach does not conflict with the Vlasov–Maxwell–Boltzmann system at fundamental level. Because ionization is the key process for sustaining the plasma it is reasonable to connect all reaction rates to ionization rate from theoretical point-of-view. This approach has been utilized in chapter 3 (publication [PI]), where the framework for the plasma heating power dissipation is presented. Light emission is both, a result of the most significant electron impact processes and a straightforwardly measurable quantity. Therefore, it is naturally a key diagnostics for this approach as presented in chapter 5 (publication [PIII]).

The probabilities of different electron impact processes can be compared by comparing their reaction rates. A volumetric reaction rate depends on the densities and velocities of the colliding particles and the cross section of the process. If the colliding particles have a large velocity difference, such as electrons in comparison to ions and neutrals, the slower particle can be assumed to be stationary. Therefore, the volumetric electron impact collision rate R with ions and neutrals can be described as

$$R = n_e\, n_n \int f_e(v)\, v\, \sigma(v)\, dv = n_e\, n_n\, \langle v\, \sigma \rangle\,, \tag{2.11}$$

where n_e is the electron density, n_n the neutral molecule density, f_e the normalized electron velocity distribution function (EVDF), v the electron velocity and σ the cross section of the process. The term $\langle v\sigma \rangle$ is the rate coefficient which depends on the functional shapes of the EVDF and the cross section. The electron velocity distribution function (EVDF) is typically presented with the electron energy distribution function (EEDF). The cross sections of different processes and EEDFs found from low temperature hydrogen plasmas are discussed in sections 2.3 and 2.4.1.

The cross sections of electron-molecule impact processes depend on the vibrational level of the molecule. In that case the total volumetric rate of a certain process can be calculated as a weighted average of the volumetric rates corresponding to individual vibrational levels. For Boltzmann vibrational distribution the result can be written as

$$R(T_{vib}) = n_n n_e \frac{\sum_i \langle v\sigma \rangle_i \exp(-\frac{E_i}{kT_{vib}})}{\sum_i \exp(-\frac{E_i}{kT_vib})} = n_n n_e \alpha(T_{vib}), \tag{2.12}$$

where T_{vib} is the vibrational temperature of the neutral gas, E_i is the energy of the vibrational level i on the ground state and $\langle v\sigma \rangle_i$ is the total excitation rate coefficient from the ground state vibrational level i to all possible vibrational levels of the upper state.

2.3 Atomic and molecular dynamics

The dynamics of the hydrogen atoms and molecules are affected both by the plasma processes and reactions on the surface of the plasma chamber. This thesis focuses on the plasma processes, which are described in this section. However, many of their reverse processes occur only on the surfaces. Therefore, surface processes are discussed briefly in section 2.3.1.

There are hundreds of different collision processes in hydrogen plasmas [25]. However, their cross sections vary by orders of magnitude and, therefore, the plasma dynamics can be understood reasonably accurately by taking into account only under 50 most significant reactions. The most significant inelastic collisions processes can be categorized to following groups:

Ionization:	e+H/H_2	$\rightarrow$	$2e$+H^+/H_2^+,
Metastable excitation:	e+H/H_2	$\rightarrow$	e+H^*/H_2^*
Radiative excitation:	e+H/H_2	$\rightarrow$	e+H/H_2 + $h\nu$
Dissociation:	e+H_2	$\rightarrow$	e+2H,
Recombination:	e+H^+/H_2^+	$\rightarrow$	H/2H+$h\nu$,
DEA[4]:	e+H_2	$\rightarrow$	H+H^-

Dynamics of the hydrogen atoms is straightforward. High energy electrons (E_e>10–15 eV) ionize and excite hydrogen atoms by electron impact. Furthermore, protons and low energy electrons can be recombined to form an atom. Cross sections of these processes are presented in Fig. 7. Hydrogen atoms are mainly produced by dissociation of hydrogen molecules by electron impact excitations. The reverse reaction, i.e. association of two hydrogen atoms, can occur only on the surface of the plasma chamber due to metastable vibrational levels of the hydrogen molecule.

The processes of the hydrogen molecule are significantly more complex than those of the atom. This is not only because higher number of processes, but also because their cross sections depend strongly on the vibrational level and several chemical processes can occur simultaneously. The cross sections of the most significant electron impact processes of the hydrogen molecule are presented Fig. 8a and their vibrational level dependence is demonstrated in Fig. 8b.

[4] Dissociative electron attachment

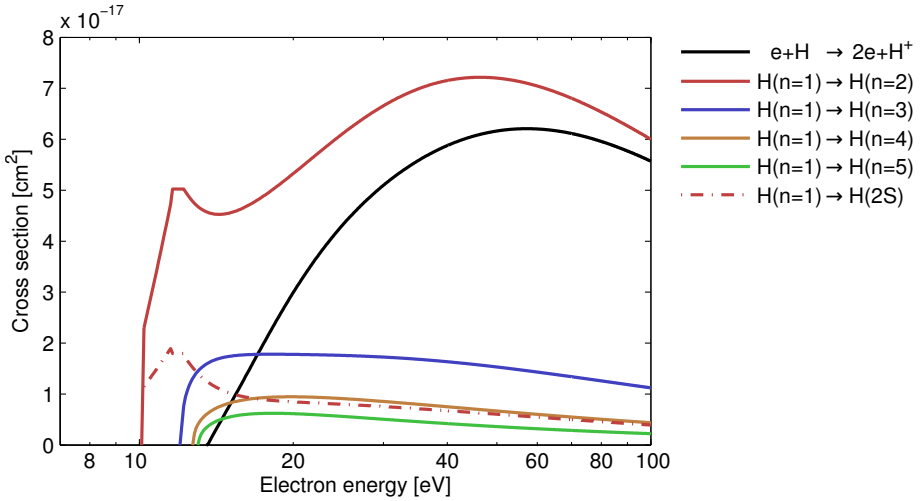

FIGURE 7 Electron impact excitation and ionization cross sections for hydrogen atom. Cross section data from Ref. [25].

The ion source performance can be optimized for the production of H^-, H^+ or H_2^+ by affecting the electron impact processes of hydrogen molecules. The main volume production mechanism of negative hydrogen ions occurs via the attractive $X^2\Sigma_u^+$ state. Cross section of this process peaks at low electron energies (E_e<4 eV) and depends by orders of magnitude on the molecule vibrational level (see Fig. 8b). Thus, the production rate of H^- ions is connected with the production rate of high vibrational levels on the ground state ($X^1\Sigma_g^+(v>5)$). The balance between H^+ and H_2^+ ions can be affected by dissociation and association rates. Furthermore, the densities of all ion species are proportional to the plasma density which in turn is affected by the ionization rate.

Molecular plasma processes can be categorized by the functional shapes of their cross sections, which is the basis of the diagnostics presented in chapter 5. Because all excitations to singlet or triplet system have similar functional shapes, the total excitation rates to the corresponding systems can be estimated from the emission bands within the system (e.g. Lyman-band for singlet and molecular continuum for triplet).

The majority of plasma chemical processes of hydrogen molecules can be connected to electronic excitations. For example, due to Franck-Condon principle vibrational excitation to high vibrational levels occurs mainly via electron impact excitations to $B^1\Sigma_u^+$ and $C^1\Pi_u$ states [52]. It can be calculated that approximately 50–60% of the $B^1\Sigma_u^+$ and $C^1\Pi_u$ excitations lead to vibrational levels v>5 independently of the plasma parameters. Furthermore, the functional shapes of the cross sections of optically allowed (singlet) excitations and ionization are similar. This means that the ionization rate is proportional to singlet emissions, e.g. Lyman-band emission.

The most significant dissociation channels of the hydrogen molecule are excitations to triplet and singlet states [25, 43]. Virtually all excitations to triplet states and 15% of excitations to $B^1\Sigma_u^+$ and $C^1\Pi_u$ lead to molecule dissociation.

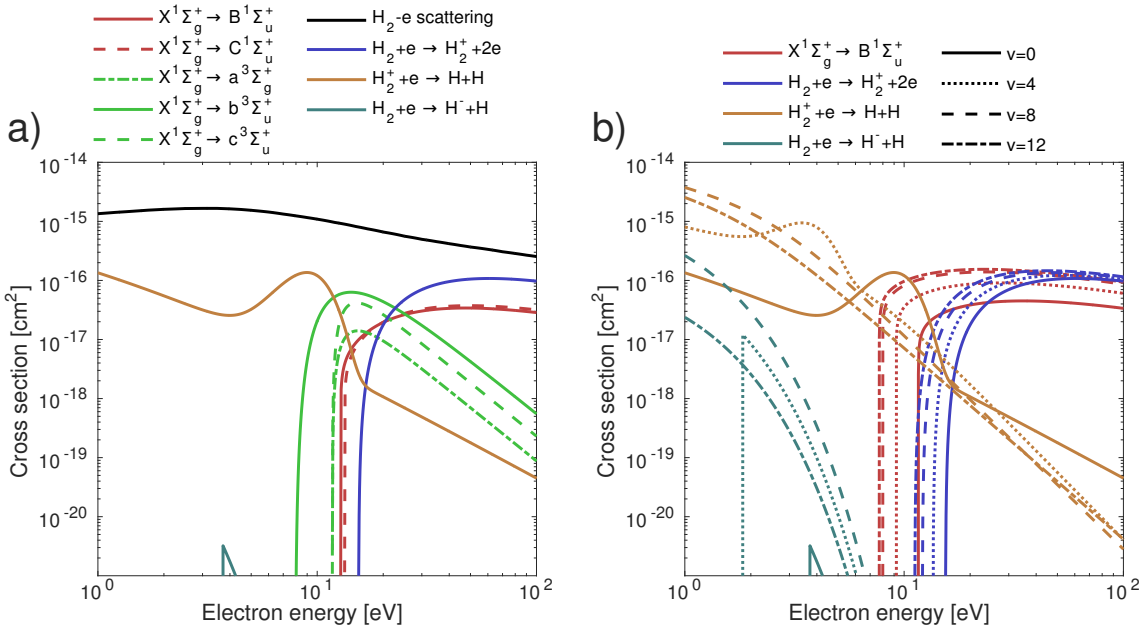

FIGURE 8 **a)** Cross sections of the most significant electron impact processes for the hydrogen molecule on the vibrational level ($\nu = 0$). **b)** Vibrational dependence of the cross sections of electronic excitation to singlet states, ionization, dissociative electron attachment and recombination. Cross section data is from Ref. [25].

Relative significance of these channels depends on the plasma parameters. Molecule dissociation via triplet states is also the most significant heating process of neutral particles due to excess kinetic energy of the resulting hydrogen atoms. Moreover, some triplet excitations produce metastable $c^3\Pi_u$ states.

Altogether this means that the singlet emission rate (e.g. Lyman-band) is proportional to the production rate of highly vibrationally excited hydrogen molecules, dissociation via vibrational continuum and ionization. Furthermore, the triplet emission (e.g. molecular continuum) is proportional to molecule dissociation via repulsive $b^3\Sigma_u^+$ state and production of metastable $c^3\Pi_u$ states.

Low temperature plasmas are heated by transferring energy to the electrons. The electron energy is transformed to photons, chemical potential and kinetic energy of other particles due to electron impact processes. Thus, another way to categorize electron impact processes is by the energy transformation. This has been utilized in the framework of the plasma heating power dissipation presented in chapter 3 (publication [PIII]).

Electron energy is transformed to photons due to excitations to electronic states. However, a part of the excitation energy of the hydrogen molecule is not converted to photon emission but to chemical potential and kinetic energy of the neutrals because of Franck-Condon principle and the existence of the repulsive $b^3\Sigma_u^+$ state. The chemical potential consists of metastable excitations to vibrational levels and electronic states and threshold energies of chemical reactions (e.g. ionization potential and dissociation energy). It can be calculated [PIII] that every singlet excitation transfers 2.3–3.1 eV of excitation energy to the chemical

potential due to Franck-Condon principle, while the rest of the excitation energy is converted to photons. Each triplet excitation transfers 4.5 eV to chemical potential due to dissociation energy of the hydrogen molecule and 1.5 eV to kinetic energy of the resulting atoms. The remaining energy of the triplet excitations is converted to photons. Metastable electronic states, namely the $2S$ atoms and $c^3\Pi_u$ molecules, carry a chemical potential of 10.2 eV and approximately 12 eV, respectively. At low electron energies direct vibrational electron impact excitation is significant energy dissipation channel.

2.3.1 Plasma-wall interaction

Particle densities are determined by the balance between production and destruction rates. Atoms, high vibrational levels and ions are produced in the plasma, but significant losses occur on the surface of the plasma chamber. Interaction between hydrogen and surfaces is still an active topic of research due to interest in astrophysics [22], thin film processing [15] and developing methods for computational surface chemistry [34]. Although the basic processes are known, there are still large uncertainties related to material dependencies of wall interactions, for example.

The most well-studied studied process is the atom association on the surfaces[5]. The probability for the hydrogen atom association varies from >10% on metal surfaces to <1% on surfaces consisting of insulating materials [15]. For example, the association probability on a copper or aluminium surface is approximately hundred times higher than on a Pyrex or alumina surface. The hydrogen molecules produced on the metal surfaces are at high vibrational levels [53].

Although, atom association has been studied extensively, reviews about material dependence of ion and highly vibrationally excited molecule interaction with the surface are not found in the literature. Some studies about the surface material effects on the performance of H^- ion sources are discussed in a recent review paper [5]. One of the few direct plasma–surface interaction experiments, performed by Gabriel et al [54], indicates that rovibrational de-excitation of H_2 molecules is a significant process on the surfaces. On the other hand, it is known that the chemical potential (e.g. ionization potential and vibrational excitation) can induce surface material excitation, electron emission, photon emission or molecule dissociation on the surface [34,55]. Development of the surface chemistry models for these processes is still an ongoing effort [34, 55]. However, it can be argued that there should be significant differences especially between metals, insulators and semiconductor materials as wall materials of the plasma chamber.

[5] Some references use term recombination for the association of the hydrogen atoms. However, in this study term recombination refers to the association of electron and ion.

2.4 Particle distributions in low temperature plasmas

Distributions of particle energies and vibrational levels in low temperature plasmas can not be typically described with the simplest distribution functions, e.g. Maxwell-Boltzmann or Boltzmann distributions. A large variation of different distributions have been found depending on the plasma parameters and mechanical design of the plasma source [13]. One of the motivations and starting points for this thesis was to develop robust plasma diagnostics and study plasma properties on a general level. This means that the developed methods and studied properties should be insensitive to variations of the particle energy distributions.

Unfortunately, there is no general, simple, way to mathematically describe the variation of particle distributions and their effect to plasma dynamics. In principle, it can be argued that this could be done by using functional calculus and Harris chains as a starting point. However, such approach is not found in the literature and is out of the scope of this thesis. Thus, distribution functions are approximated as a combination of ideal distribution functions. The chosen approach is justified in this section.

Electron energy distribution and vibrational distribution of neutral molecules affect the plasma dynamics in low temperature plasmas most significantly. These distributions will be described precisely in the following sections 2.4.1 and 2.4.2. Also (kinetic) energy distributions of neutrals and ions are typically non-Maxwellian (see e.g. [56]). However, they are omitted due to negligible effects to reactions and dynamics described herein.

2.4.1 Electron energy distribution

The electron energy distribution function (EEDF) is a result of collision processes, electron heating and plasma confinement. Electron energy distribution functions have been studied intensively both experimentally and numerically. There are numerous experimental studies of EEDFs based on Langmuir-probe measurements (see e.g. Ref. [13]) or optical emission spectroscopy (see e.g. Ref. [57]). However, only a few of them cover precisely the hot electrons which are responsible for ionization and electronic excitation of the neutral gas. The majority of numerical studies is based on solving the Boltzmann equation (see e.g. Ref. [58]). Particle-in-cell–Monte-Carlo (PIC-MC) simulations, which provide spatial information about the EEDF have also been developed (see e.g. Ref. [59]). However, there is a lack of experimental data for benchmarking and validating the results given by the simulation codes.

The plasma confinement affects the EEDF in three different ways. Because of significant velocity and mass difference of electrons and ions, the plasma is driven to positive electric potential with respect to the plasma chamber in order to balance electron and ion fluxes to the wall. Due to high electric conductivity of the plasma, the potential difference, namely plasma potential, builds up in a thin sheet close to the wall. This plasma potential confines electrons whose energy

is less than the energy required to exceed the plasma potential. The magnitude of the plasma potential depends on the magnetic confinement, plasma heating and neutral gas pressure. Increasing the average energy of the electrons increases the plasma potential. In contrast, the magnetic field lowers the plasma potential due to reduced electron diffusion (in comparison to ions) in the direction perpendicular to the magnetic field. The diffusion is proportional to electron collision rate.

The magnetic field affects the EEDF also due to magnetic confinement. The electrons are confined in the direction of the magnetic field by the magnetic mirror effect, which means that charged particles are reflected stronger field towards weaker field. The process depends on the ratio of perpendicular and parallel velocity components of the electron with respect to the magnetic field. Electrons are reflected (confined) if the following condition holds:

$$\frac{v_\perp}{v} > \sqrt{\frac{B_{\min}}{B_{\max}}}, \tag{2.13}$$

where $v_\perp$ is the perpendicular velocity component at the minimum magnetic field strength $B_{\min}$, v is the total velocity of the electrons and $B_{\max}$ is the maximum magnetic field strength. The electron mean free path between collisions is often comparable or longer than the dimensions of the low temperature plasma sources. This means that the confinement of the electrons with high $\frac{v_\perp}{v}$ is determined by stochastic collisional diffusion to lower $\frac{v_\perp}{v}$. Although the magnetic mirror effect itself does not depend on the total energy of the electron, the collision rate depends strongly on the electron energy, i.e. the total collision rate decreases with increasing electron energy. Thus, the magnetic confinement of the cold electrons is weaker with respect to the hot electrons.

Significance of different collision processes of the electrons depend on the plasma parameters, especially the electron energy and ionization degree. The dominating process for the low energy electrons (E_e<8 eV) is Coulomb collisions, i.e. elastic electron-electron and electron-ion collisions. Furthermore, in the case of molecular hydrogen plasma the low energy electrons excite molecules vibrationally and produce negative hydrogen ions via dissociative electron attachment. The most significant collision processes for high energy electrons (E_e>8 eV) at low ionization degree are ionization and electronic excitation of the neural gas.

The EEDF is, by definition, Maxwellian when electron-electron coulomb collisions dominate in the entire electron energy range. This is typically valid only for the low energy part of the EEDF (E_e<8 eV). The high energy part of the EEDF represents a balance between inelastic collisions and plasma heating. As a result bi-Maxwellian distributions are typically found at low pressures and/or when high plasma heating power is applied [13]. Meanwhile, Druyvesteyn-like distributions have been found at high pressures [13]. Furthermore, superpositions of Maxwellian and uniform (or flat) distributions have been commonly found in filament arc discharges (e.g. Refs. [60–62]).

Maxwellian, Druyvesteyn and uniform distributions have been chosen for a closer study in this thesis. Those distributions represent the mathematical varia-

tion found in laboratory plasmas in terms of the variation of rate coefficients. The Maxwellian and Druyvesteyn distributions can be described with the equation

$$f(E_e) = \alpha\sqrt{E_e}\exp\left[-\beta\left(\frac{E_e}{k_b\,T_e}\right)^{\gamma}\right], \tag{2.14}$$

where k_b is the Boltzmann constant, T_e is the effective electron temperature, α is the normalization factor and β and γ are distribution-specific coefficients [57]. The coefficients β and γ are 1 for the Maxwellian distribution while they are 0.24 and 2 for the Druyvesteyn distribution respectively.

The uniform distribution can be presented as

$$f(E_e) = \begin{cases} \alpha & \text{if } E_e \leq E_{max} \\ 0 & \text{if } E_e > E_{max} \end{cases} \tag{2.15}$$

where α is the normalization factor and E_{max} is the endpoint (or maximum) energy of the plasma electrons corresponding to the potential difference between the cathode and the plasma.

The plasma diagnostics method presented in chapter 5 is based on the comparison of the rate coefficients. The discussed processes (i.e. ionization and electronic excitation) are only sensitive to hot electrons (E_e>8 eV) due to high threshold energies. The accuracy of the diagnostics partially depends on the sensitivity of the rate coefficients ratio on the variation of the EEDF. In order to demonstrate the insensitivity of the diagnostic on such variations, mathematical functions which represent the largest variation at high electron energies are required. Boltzmann and uniform distributions were chosen for this purpose. At high energies the Maxwellian distribution and the tail of the bi-Maxwellian distribution can be described by the Boltzmann probability function

$$f(E_e) = \alpha\exp\left(-\frac{E_e}{k_b\,T_e}\right). \tag{2.16}$$

The high-energy tail of the EEDF in filament arc discharges can be described by the uniform distribution presented in equation 2.15

2.4.2 Vibrational distribution

The ideal vibrational distribution is a result of thermal collisions between hydrogen molecules. It results to the Boltzmann distribution of vibrational levels, which can be written as

$$f(\nu) = \alpha\exp\left(-\frac{E_\nu}{k_b T_{vib}}\right), \tag{2.17}$$

where α is the normalization factor, E_ν is the energy of the vibrational level ν and T_{vib} is the vibrational temperature. Plasma processes and plasma-wall interaction affect vibrational levels and, therefore, the vibrational distribution of low temperature hydrogen plasmas deviates from the Boltzmann distribution. Typically there are more molecules at high vibrational levels than could be expected

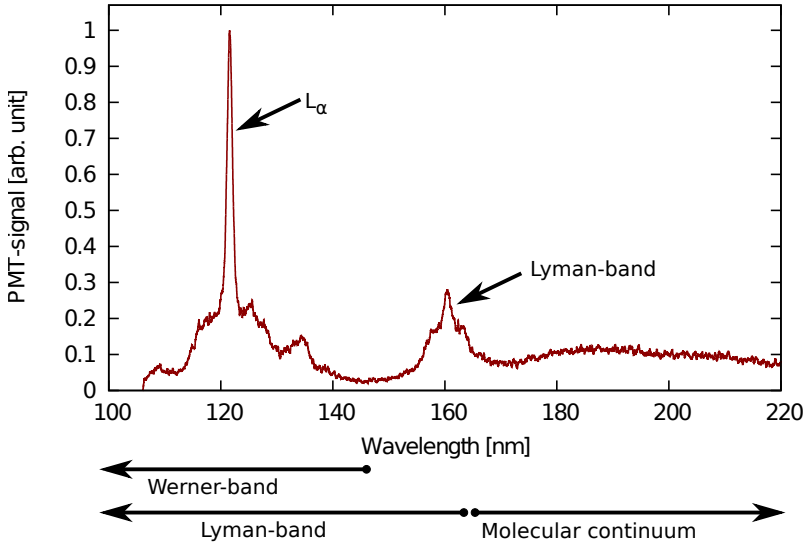

FIGURE 9 VUV spectrum of the LIISA ion source. The spectrum is not calibrated for spectral response. The resolution of the spectrometer is approximately 1.5 nm. Figure is from Ref. [PIII].

for Bolzmann equilibrium [63]. This difference is due to non-thermal reactions, i.e. electronic excitations to $B^1\Sigma_u^+$ and $C^1\Pi_u$ states and plasma–wall interaction discussed in section 2.3.

The population of high vibrational levels affects significantly the processes whose cross sections depend on the vibrational level by orders of magnitude. This kind of process is, for example, the volume production of negative hydrogen ions (dissociative electron attachment). However, the cross sections of the processes studied in this thesis, such as electronic excitations and ionization, are less than linearly proportional to the vibrational level. Typically, the majority (>90%) of neutral molecules are on the lowest vibrational levels (v<4) (see e.g. summary of distributions in Ref. [63]). This population can be described reasonably well with the Boltzmann distribution in the 100–10000 K vibrational temperature range. Thus, in this thesis the variation of the rate coefficients caused by the varying vibrational distribution is modelled using Boltzmann distribution in the range of 100–10000 K.

2.5 Vacuum ultraviolet spectrum of hydrogen plasmas

A typical vacuum ultraviolet (VUV) spectrum of a low temperature hydrogen plasma is presented in Fig. 9. It is a superposition of the atomic emission (Fig. 2) and molecular emission (Fig. 5). Lyman-alpha ($2P \rightarrow 1S$) at 121.6 nm is emitted by the lowest transition of the hydrogen atom. The molecular emission originates from the lowest transitions of the hydrogen molecule, namely Lyman-band ($B^1\Sigma_u^+ \rightarrow X^1\Sigma_g^+$), Werner-band ($C^1\Sigma_u^+ \rightarrow X^1\Sigma_g^+$) and molecular continuum ($a^3\Sigma_g^+ \rightarrow b^3\Sigma_u^+$).

The molecular photon emission rate corresponds to the electron impact excitation rate in corona equilibrium. Low temperature laboratory plasmas are optically thin for the molecular emission due to Franck-Condon principle. The origin of the atomic emission is more complex, because atoms can be excited directly by electron impact or emission can be due to dissociative excitation of the molecule, e.g. due to electronic excitation to vibrational continuum or recombination of molecular ions [25]. Moreover, resonance photon excitation of atoms, could have a significant effect on the transmission of the atomic emission in the plasma [64].

Lyman-band and molecular continuum emissions are suitable transitions for diagnostic purposes of plasma processes. This is because their origin can be understood straightforwardly and wavelength ranges of 145–170 nm and 170–230 nm consist predominantly of Lyman-band and molecular continuum emissions, respectively. However, the emissions are partially caused by cascade from the upper states and wavelength ranges of 145–170 nm and 170–230 nm do not cover the entire emission bands of Lyman-band and molecular continuum due to Franck-Condon principle explained in Section 2.1.2 . The total photon emission rate of the Lyman-band and molecular continuum can be estimated from

$$R_{tot} = \frac{R_{meas}}{k_{cov}} k_{cas}, \tag{2.18}$$

where R_{meas} is the measured photon emission rate of the partial emission band, k_{cov} is the correction coefficient for the coverage of the emission band and k_{cas} is the correction coefficient for the cascade effect from the upper states.

The values of k_{cov} and k_{cas} can be studied by producing a synthetic spectrum as described in publications [PII] and [PIII]. The first order approximation is that vibronic transitions in electron impact excitations follow the Franck-Condon factors. This assumption is widely used [30], but not completely accurate. Vibrational transition probabilities in electron impact excitations are affected also by the varying threshold energy and cross section for different transitions, which can change the situation significantly especially at low electron energies [65].

The synthetic spectrum produced with the Franck-Condon factors depends only on the vibrational temperature of the plasma. By using the typical vibrational temperature range of 100–10000 K, it can be calculated that the wavelength range 145–170 nm covers 38–43% of the total Lyman-band emission [PIII]. The synthetic spectrum presented in Ref. [65] yields that the range of 170–240 nm covers 59–62% of the total molecular continuum emission.

The lowest singlet state, $B^1\Sigma_u^+$ is partially populated by cascade from the upper states (see Fig. 4). The cascade effect has been studied intensively and the latest study yields that on average 15% of the Lyman-band emission is caused by the cascade from the upper states [66].

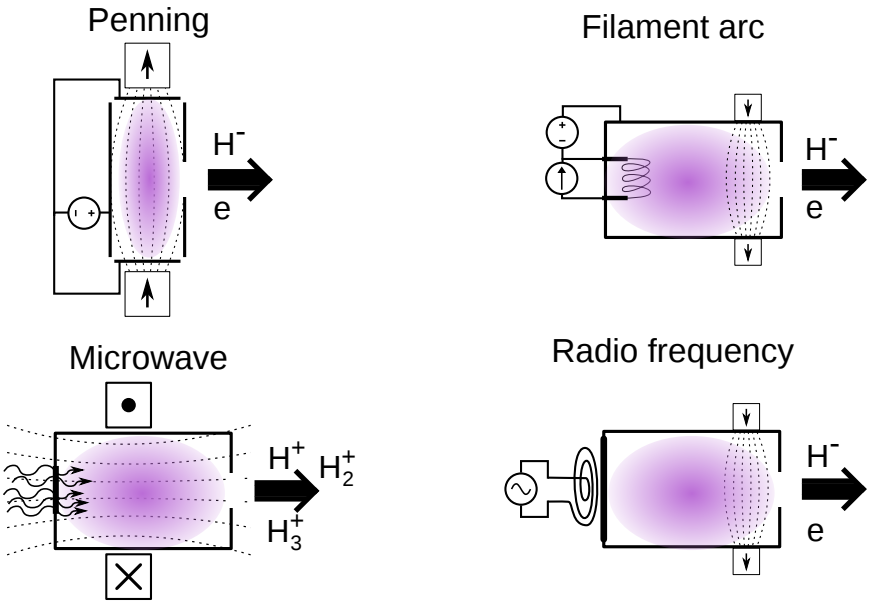

FIGURE 10 Schematic picture of different types of hydrogen ion sources. Plasma is indicated with magenta and the dashed lines correspond to magnetic field lines.

2.6 Plasma ion sources

The main principle of plasma ion sources is to produce a plasma consisting of required ions and extract them through an aperture in the plasma chamber. The ions are extracted by utilizing high voltage electrodes. Production of all hydrogen ions (H^-, H^+ and H_2^+) requires warm, ionizing, plasma. Positive hydrogen ions are extracted directly from the warm plasma [46], but magnetically filtered tandem ion sources have been developed for negative ions [52]. This is because the negative hydrogen ions are are susceptible to dissociation in collisions and their extraction is complicated by co-extracted electrons. The tandem ion source consists of two plasma regions. Dense and warm plasma in the driver region produces electrons and highly vibrationally excited molecules while the negative hydrogen ions are produced during plasma diffusion through a transverse magnetic field in the extraction region. The plasma diffusion through the magnetic filter field reduces also the fraction of co-extracted electrons.

Hydrogen ions are produced with numerous types of plasma sources [46, 67]. These plasma sources can be categorized to three different groups based on the plasma heating method: hot cathode, cold cathode and electromagnetic wave -driven sources. Hot cathode plasma sources, such as filament driven arc discharges, are sustained by high energy electrons emitted from the hot cathode surfaces. The electrons are accelerated in thin plasma sheath and subsequently dissipate their energy in the plasma. Cold cathode plasma sources are sustained only by potential difference between two electrodes. Plasma breakdown and maintenance of a cold cathode discharges is complex balance of plasma processes

as described for argon discharges in Ref. [68]. Plasma electrons can be heated with electromagnetic waves in a wide frequency range from radiowaves (1 MHz) to microwaves (>10 GHz). There are still uncertainties related to exact heating mechanisms of the radio frequencies (RF) as discussed in Ref. [69]. Regular consensus is that RF heating in capacitive mode occurs collisionlessly in the sheat caused by varying RF electric field, while in the inductive mode heating occurs due to varying electromagnetic field induced by alternating coil current [13].The RF antenna can be either external [70,71] or it can be immersed in the plasma [72].

At microwave frequencies (>1 GHz) the plasma is typically heated with electron cyclotron resonance (ECR) [13]. The ECR heating is a resonance phenomenon which occurs when the electron gyrofrequency in the magnetic field is equal to the frequency of injected microwaves. 2.45 GHz microwaves produced by magnetron generators are often used for plasma heating. Fulfilling the resonance condition at this frequency requires a magnetic field strength of 87.5 mT. However, it has been demonstrated that efficient microwave heating occurs also without satisfying the ECR conditions and even without external magnetic field (see e.g. Ref. [73] and references therein).

Modern proton sources are commonly based on 2.45 GHz microwave discharges [74]. The majority of negative hydrogen ion sources are based on the tandem design [52, 67]. Most of the operational H^- ion sources utilize filament driven arc discharge or RF heating while the plasma confinement is improved with a multicusp magnetic field. The experimental part of this thesis consists of measurements with a 2.45 GHz microwave ion source and filament driven arc discharge H^- ion source, LIISA. Detailed descriptions of these ion sources are presented in sections 4.1 and 4.2.

Due to the technical benefits of microwave discharges in comparison to filament driven and RF discharges, several attempts have been made in the past to apply microwave heating for the production of negative hydrogen ions. The earliest study was performed by Hellblom and Jacquot [75] using 11 GHz electron cyclotron resonance (ECR) heating in solenoid magnetic field. This pioneering experiment has been followed in several studies utilizing different technical solutions [73, 76–80]. The most recent results from Peng et al. [81] are promising, but the long-awaited breakthrough is still missing.

Performance of the ion source and relevance of different plasma processes are directly connected to the plasma heating method and mechanical design of the ion source. This is due to dynamics of the hydrogen atoms and molecules, plasma-wall interactions and EEDF as discussed in Sections 2.3 and 2.4. However, a good example of the effects of mechanical design on the ion source performance is not found in the literature. A reason for this could be the lack of necessary diagnostics, which is the topic of this thesis. Thus, a more detailed discussion about technical aspects affecting the ion source performance is presented in chapter 6.

3 PLASMA HEATING POWER DISSIPATION

Low temperature plasmas are heated and sustained by transferring energy to the electrons. The electrons dissipate their energy to light emission, chemical potential and kinetic energy of ions in inelastic electron impact collisions. All of these power dissipation channels carry the heating power to the walls of the plasma chamber. The only directly measurable power dissipation channel is photon emission.

Studies of plasma heating power dissipation are rarely found from the literature. Batishchev et al. studied a helicon discharge with plasma simulations and found that approximately 25% of the discharge power dissipates via photon emission [9]. In principle, information about photon emission could be extracted from commonly used plasma simulation models (see details of the models e.g. from Refs. [47,49,63,82]). Unfortunately, such information has not been reported and on the other hand, generalizing the results is challenging due to unique mechanical designs of the simulated plasma sources.

From the plasma physics point of view, applying classical models, such as Boltzmann equilibrium and Saha equation, require unrealistic assumptions that are questionable in the case of laboratory plasmas. On the other hand, radiative condensation models describe only nonlinear dynamics of instabilities [83] and excimer light source models cover only the energy transfer from electrons to neutral gas [84]. The collisional energy loss per created electron–ion pair is commonly used parameter in the literature [13], but it is not utilized for the analysis of the heating power dissipation.

A framework for plasma heating power dissipation in low temperature plasmas is developed in this study (publication [PI]). The framework focuses only on the power dissipation and, therefore, it is significantly simpler than most commonly used simulations [47, 49, 82]. As a result, the power dissipation can be studied at a general level, the uncertainties can be understood and some predictions can be made. This chapter describes a summary of the heating power dissipation framework, which is presented more accurately in publication [PI].

The approach is based on elementary principles of physics and low temperature plasmas:

1. Heating power is transferred to electrons with the first step of the power dissipation being inelastic electron impact collisions
2. It is always possible to calculate the ratio of specific volumetric reactions
3. The electric charge, mass and energy are conserved.
4. The local change or flux of a quantity can be described with the general continuity equation (divergence theorem)

$$\frac{\partial n_\alpha}{\partial t} + \nabla \cdot \boldsymbol{j}_\alpha = r_\alpha, \tag{3.1}$$

where $\frac{\partial n_\alpha}{\partial t}$ is the rate of density change, $\boldsymbol{j}$ is the flow and r is the volumetric generation rate of the quantity α

The total energy of the plasma can be divided to kinetic energy of particles, chemical potential and energy carried by electromagnetic fields. The energy of the electromagnetic fields can be divided into photons and electromagnetic waves based on their interactions with the plasma. Photons interact with individual plasma particles, while electromagnetic waves interact collectively with charged particles. The conservation of energy requires that the rate of energy density change is the sum of divergences of different energy fluxes, i.e

$$-\frac{\partial u_{\text{tot}}}{\partial t} = \nabla \cdot \boldsymbol{S}_{\text{k}} + \nabla \cdot \boldsymbol{S}_\mu + \nabla \cdot \boldsymbol{S}_{\text{em}} + \nabla \cdot \boldsymbol{S}_\nu, \tag{3.2}$$

where $\boldsymbol{S}_{\text{k}}$ is the kinetic energy flux density of the particles, $\boldsymbol{S}_\mu$ is the chemical potential flux density carried by the particles, $\boldsymbol{S}_{\text{em}}$ is the energy flux density of electromagnetic waves and $\boldsymbol{S}_\nu$ is the energy flux density of photons.

The energy density in the steady state of an open thermodynamic system is constant. This means that absorbed (plasma heating) power correspond to outgoing energy flow. In the low temperature plasmas escaping energy is carried by photons ($\nabla \cdot \boldsymbol{S}_\nu$), chemical potential ($\nabla \cdot \boldsymbol{S}_\mu$) and kinetic energy of the particles ($\nabla \cdot \boldsymbol{S}_{\text{kp}}$), i.e.

$$P_{\text{heat}} = \nabla \cdot \boldsymbol{S}_{\text{heat}} = \nabla \cdot \boldsymbol{S}_\nu + \nabla \cdot \boldsymbol{S}_\mu + \nabla \cdot \boldsymbol{S}_{\text{kp}}, \tag{3.3}$$

Thus, the (local) power dissipation to photons (P_ν), ionization (P_{inz}) and chemical potential (excluding ionization) ($P_{\mu c}$) can be expressed as

$$\frac{P_\nu}{P_{\text{heat}}} = \frac{\nabla \cdot \boldsymbol{S}_\nu}{\nabla \cdot \boldsymbol{S}_\nu + \nabla \cdot \boldsymbol{S}_\mu + \nabla \cdot \boldsymbol{S}_{\text{kp}}} \tag{3.4}$$

$$\frac{P_{\text{inz}}}{P_{\text{heat}}} = \frac{\nabla \cdot \boldsymbol{S}_{\text{inz}}}{\nabla \cdot \boldsymbol{S}_\nu + \nabla \cdot \boldsymbol{S}_\mu + \nabla \cdot \boldsymbol{S}_{\text{kp}}} \tag{3.5}$$

$$\frac{P_{\mu c}}{P_{\text{heat}}} = \frac{\nabla \cdot \boldsymbol{S}_{\mu c}}{\nabla \cdot \boldsymbol{S}_\nu + \nabla \cdot \boldsymbol{S}_\mu + \nabla \cdot \boldsymbol{S}_{\text{kp}}} \tag{3.6}$$

Electron impact processes are discrete events and, therefore, the rate of change of the energy density can be expressed as

$$\nabla \cdot \boldsymbol{S}_\alpha = \langle E_\alpha \rangle \, R_\alpha, \tag{3.7}$$

where $\langle E_\alpha \rangle$ is the average dissipated energy and r_α is the volumetric reaction rate of the process α.

Ionization is the primary process for sustaining the plasma due to finite electron and ion confinement time. Therefore, it is rational to connect the rates of energy density changes through different reaction mechanisms to the energy used for ionization. Volumetric reaction rates r_α can be expressed with the volumetric ionization rate r_{inz} by

$$r_\alpha = \frac{R_\alpha}{R_{\text{inz}}} r_{\text{inz}} \equiv k_\alpha R_{\text{inz}}. \tag{3.8}$$

Thus, the divergences of the energy flux densities in equations 3.4–3.6 can be written as

$$\nabla \cdot \boldsymbol{S}_\alpha = k_\alpha \, \langle E_\alpha \rangle \, R_{\text{inz}}, \tag{3.9}$$

where k_α is the ratio of the volumetric rates of process α and ionization. Only electron impact processes of neutral particles are studied in this thesis, which means that the ratios, k_α, depend only on the rate coefficients $\langle \sigma v \rangle$, i.e.

$$k_\alpha = \frac{R_\alpha}{R_{\text{inz}}} = \frac{n_e n_n \langle \sigma v \rangle_\alpha}{n_e n_n \langle \sigma v \rangle_{\text{inz}}} = \frac{\langle \sigma v \rangle_\alpha}{\langle \sigma v \rangle_{\text{inz}}}. \tag{3.10}$$

Hence, Eqs. 3.4–3.6 do not depend on the reaction rates themselves but only on the cross sections determined by the gas species and the average electron energy , which affect the ratios of the rate coefficients, the ratio of volumetric recombination and ionization rates ($\frac{R_{\text{rec}}}{R_{\text{inz}}}$) and the average energy of escaping electron–ion pair produced in the plasma volume, $\langle \Delta E_p \rangle$. This yields

$$\begin{aligned} \frac{P_\nu}{P_{\text{heat}}} &= \left(k_{\nu\text{e}} \langle E_{\nu\text{e}} \rangle + \langle E_{\nu\text{r}} \rangle \frac{R_{\text{rec}}}{R_{\text{inz}}} \right) \\ &/ \left(k_{\nu\text{e}} \langle E_{\nu\text{e}} \rangle + k_{\mu c} \langle \Delta E_{\mu c} \rangle + k_{\text{kn}} \langle \Delta E_{\text{kn}} \rangle + E_{\text{inz}} \right. \\ &\left. + \langle \Delta E_p \rangle + (\langle E_{\nu\text{r}} \rangle - E_{\text{inz}} - \langle \Delta E_p \rangle) \frac{R_{\text{rec}}}{R_{\text{inz}}} \right), \end{aligned} \tag{3.11}$$

$$\begin{aligned} \frac{P_{\text{inz}}}{P_{\text{heat}}} &\geq \left(E_{\text{inz}} (1 - \tfrac{R_{\text{rec}}}{R_{\text{inz}}}) \right) \\ &/ \left(k_{\nu\text{e}} \langle E_{\nu\text{e}} \rangle + k_{\mu c} \langle \Delta E_{\mu c} \rangle + k_{\text{kn}} \langle \Delta E_{\text{kn}} \rangle + E_{\text{inz}} \right. \\ &\left. + \langle \Delta E_p \rangle + (\langle E_{\nu\text{r}} \rangle - E_{\text{inz}} - \langle \Delta E_p \rangle) \frac{R_{\text{rec}}}{R_{\text{inz}}} \right). \end{aligned} \tag{3.12}$$

$$\frac{P_{\mu c}}{P_{\text{heat}}} \leq \left(k_{\mu c}\left\langle \Delta E_{\mu c}\right\rangle\right) \Big/ \Big(k_{\nu \text{e}}\left\langle E_{\nu \text{e}}\right\rangle + k_{\mu c}\left\langle \Delta E_{\mu c}\right\rangle + k_{\text{kn}}\left\langle \Delta E_{\text{kn}}\right\rangle + E_{\text{inz}} + \left\langle \Delta E_p\right\rangle + \left(\left\langle E_{\nu \text{r}}\right\rangle - E_{\text{inz}} - \left\langle \Delta E_p\right\rangle\right)\frac{R_{\text{rec}}}{R_{\text{inz}}}\Big). \tag{3.13}$$

where E_{inz} is the ionization potential and subscript ve refers to the photon emission due to electron impact excitation, vr refers to the photon emission due to recombination, μc refers to the chemical potential and kn refers to the kinetic energy of neutral particles.

The powers related to photon emission, ionization and chemical potential calculated with equations 3.11–3.13 do not correspond to outgoing powers, if there are destructive processes in the plasma volume. The destructive processes depend strongly on the plasma parameters. Low temperature plasmas are typically optically thin, i.e. destructive processes of photons are negligible. In typical hydrogen discharges the majority of metastable states escape from the plasma [38]. Their most significant de-excitation processes are radiative decay induced by collisions and ionization [85]. Thus, assuming that the de-excitation of metastable states is negligible corresponds to minimum photon emission, minimum ionization and maximum chemical potential. Typical laboratory plasmas [52, 86] are ionizing, i.e. recombination rate is negligible in comparison to ionization rate, $\frac{R_{\text{rec}}}{R_{\text{inz}}}$=0. The condition $\frac{R_{\text{rec}}}{R_{\text{inz}}}$=0 corresponds to minimum photon emission power and maximum ionization power, because in recombination the electron energy is transferred dominantly to photon emission.

The ratio of the average energies of the escaping electron-ion pair and the kinetic energy of the plasma electrons $\beta=\frac{\langle \Delta E_p\rangle}{\langle E_e\rangle}$ can be used as a parameter to describe the minimum photon emission. The plasma potential does not directly affect β, because its effect on electron and ion kinetic energies is opposite. However, it effectively increases β by determining the minimum energy of escaping electrons. The ratios $\frac{P_\nu}{P_{\text{heat}}}$ and $\frac{P_{inz}}{P_{\text{heat}}}$ are presented in Fig. 11 as a function of the average electron energy and parameter β.

The results of Eqs. 3.11–3.13 can be calculated for various EEDFs as presented in Fig. 11. It can be justified that the EEDFs presented in section 2.4.1 represent the mathematical functional variation of the real EEDFs found in laboratory plasmas. Therefore, the fractions of plasma heating power dissipation in any (infinitesimal) volume element of the plasma can be described by the curves in Figs. 11a and 11b. The relevance (fraction) of each power dissipation channel varies spatially in the finite plasma volume due to spatially varying EEDF. However, because the variation of the power dissipation fraction is represented by continuous functions, the mean value theorems for integrals govern that volumetric average of the values is found at certain local values. This means that, the fractions of the plasma heating power dissipation in specific points (corresponding to a certain EEDF) can be used to describe the fractions of plasma heating

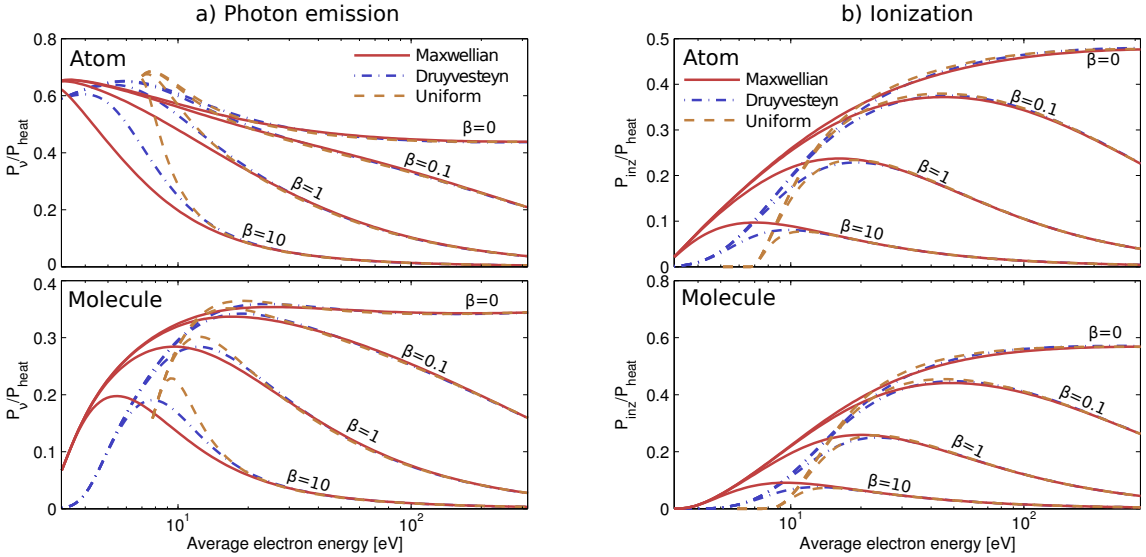

FIGURE 11 Fraction of plasma heating power converted to photon emission (a) and dissipated in ionization (b) as a function of the average electron energy for different EEDFs. The parameter β corresponds to the ratio of the escaping electron-ion pair energy to the average electron energy in the plasma. Figures are from Ref. [PI].

power dissipation in the entire plasma volume[1]. This allows drawing some conclusions from Eqs. 3.4–3.6 (Figs. 11a and 11b) as basic properties of low temperature hydrogen plasmas:

1. At least 10% of the plasma heating power is dissipated via photon emission when at least 1% of the heating power is dissipated in ionization ($\frac{P_{\text{inz}}}{P_{\text{heat}}}$>0.01). The result is independent of the plasma confinement (β) at low average electron energies ($\langle E_e \rangle$<20 eV).
2. At least 15–70% of the heating power is dissipated via photon emission, when at least 10% of heating power is dissipated in ionization.
3. The efficiency of plasma heating can be described as a fraction of power used for ionization, $\frac{P_{\text{inz}}}{P_{\text{heat}}}$ (Fig. 11). The maximum of plasma heating efficiency is achieved when $\langle E_e \rangle \geq 10$ eV the independent of the plasma confinement (β)
4. The chemical potential related to dissociation and excitation to metastable states decreases with increasing average electron energy. At low average electron energies ($\langle E_e \rangle \leq 5$ eV) the majority of the heating power is converted to chemical potential in molecular plasmas. This is mostly due to molecule dissociation through excitation to the lowest (repulsive) triplet state and direct vibrational excitation.
5. The relevance of each power dissipation channel is independent of the functional shape of the EEDF, if the average electron energy exceeds 20 eV

[1] The specific point is typically found in the hot (central) region of the plasma source, where most of the inelastic electron collisions occur.

In an ideal plasma source (good plasma confinement) the kinetic energy of the electron-ion pair is minimal in comparison to the average electron energy, i.e. β=0. In other words the electron energy is efficiently dissipated in inelastic collisions before they escape the confinement. This situation is typical in filament driven multicusp arc discharges [13] which allows some additional conclusions to be drawn:

1. Plasma heating efficiency, $\frac{P_{\text{inz}}}{P_{\text{heat}}}$, increases as a function of the average electron energy and the maximum is limited to 45–60%
2. At least 30% of the heating power dissipates via photon emission, when the plasma heating efficiency is high ($\frac{P_{\text{inz}}}{P_{\text{heat}}}$>0.4)
3. The plasma heating efficiency ($\frac{P_{\text{inz}}}{P_{\text{heat}}}$) saturates when $\langle E_e \rangle$>50 eV (E_{max}>100 eV)

4 APPARATUS FOR ABSOLUTE VUV-EMISSION MEASUREMENTS

Vacuum ultraviolet spectroscopy of plasmas is actively used for research of magnetic confinement fusion and development of plasma sources for thin film processing. One of the the primary challenges in magnetic confinement fusion are radiation condensation instabilities, which are primarily caused by VUV/EUV radiation emitted by impurities [87, 88]. They transfer significant amount of the energy stored of the plasma to (VUV) photon emission and result to plasma cooling. There is also need for intensive VUV-sources in photolithography [89, 90] for which specific plasma sources have been developed (see e.g [91]).

VUV-emission is typically measured with spectrometers consisting of a monochromator and a photomultiplier tube. These devices are practical for relative spectral measurements. However, their calibration for absolute irradiance is extremely challenging. In standard VUV spectrometer systems only a single optical element is employed to minimize absorption losses. Such spectrometer is far from ideal optical system which means that the calibration of the system is valid only for the specific source geometry and wavelength considered during the calibration procedure [10].

Spectrometers are typically calibrated by using calibrated lamps as a reference. These calibration lamps are typically point sources, which is fundamentally different from the finite line of sight plasma volume of most ion sources. In order to minimize geometrical effects alternative calibration methods have been developed for thermonuclear fusion research, such as branching pair technique [92] and bremsstrahlung continuum [11]. These techniques utilize special properties of thermonuclear fusion plasmas and, therefore, applying them for low temperature plasmas is virtually impossible.

Another approach for absolute VUV measurements is to use factory calibrated photodiode and optical filters. VUV-sensitive photodiode and optical windows have been utilized for this purpose, for example, in thermonuclear fusion research [93] and development of eximer lamps [94]. The irradiance can be calculated from the measured current signal, when the spectral response of the diode, transmittances of the filters and the effective area of the photodiode are

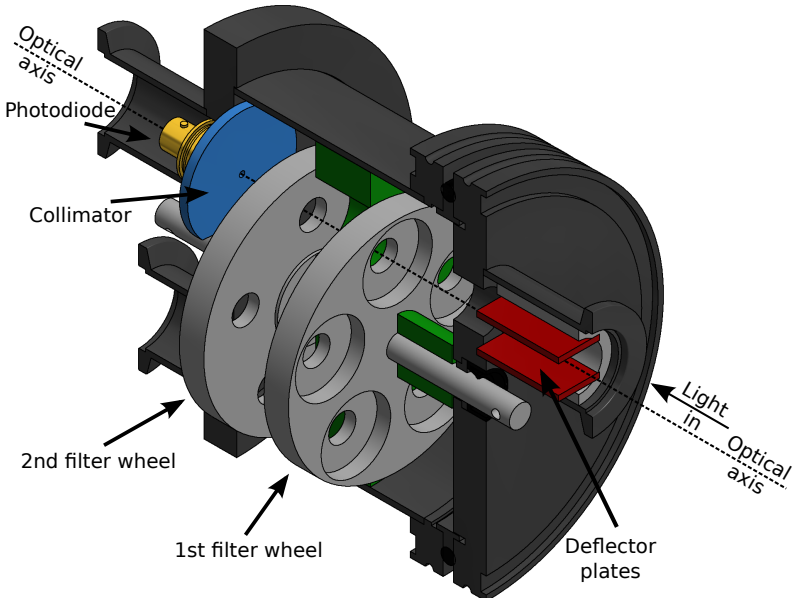

FIGURE 12 Main parts of the spectral irradiance meter. The meter can be connected to a VUV-spectrometer after removing the collimator and the photodiode. Figure is from Ref. [PII].

known. This method is robust, because geometrical effects can be understood straightforwardly. Disadvantages are lower spectral resolution, increased number of sources of uncertainty and the fact that accurate determination of the effective transmittances requires knowledge about the plasma emission spectrum due to non uniform transmission of the filters.

The measurements in this study were performed with apparatus presented in Fig. 12. The device is based on a photodiode and optical filters (publication [PII]). The apparatus consists of a vacuum chamber, two rotatable wheels for optical filters, a VUV-sensitive photodiode and high voltage plates for deflecting charged particles (possibly) incident from the plasma. The wheels are rotated externally via vacuum feedthroughs. The meter can be connected to different types of vacuum systems and spectrometers through DN25KF flanges. The photoelectric current was measured from a photodiode (IRD SXUV5) by using SRS SR570 current preamplifier. The effective area of the photodiode was restricted by a $\varnothing 2$ mm collimator aperture, because a constant response is guaranteed only at the center of the diode.

The total VUV-emission at 80–350 nm wavelengths and the characteristic VUV-emission bands of hydrogen (see section 2.5) were measured. The total emission in 80–280 nm wavelength range was determined by comparing signals measured without and with UV-FS/BK7 windows. Because UV-FS and BK7 windows are transparent in the range of 170–2000 nm and 350–2000 nm respectively and the response of IRD SXUV photodiode is uniform in the range of 80–280 nm the total VUV-emission in the range of 80–170 nm/80–350 nm is linearly proportional to the signal difference. The VUV-emissions of characteristic bands were measured by using optical band pass filters for Lyman-alpha/Werner band

(122 nm, FWHM 20 nm), Lyman-band (160 nm, FWHM 20 nm) and Molecular continuum (180 nm, FWHM 40 nm). The band pass filters were located in the second filter wheel.

The first filter wheel included both a 3 mm thick uncoated UV fused silica and BK7 windows and an aluminium plate. These were used for the measurements of background signals caused by scattering inside the meter and extremely low but measurable visible light transmittance of the band pass filters. The background signal level was negligible in the measurements from the microwave discharge but thermal radiation of filaments in the case of the filament driven arc discharge source caused a significant background signal.

Irradiance E on the photodiode can be calculated from the measured current i with

$$E = \frac{i}{A_d R \tau_\mathrm{f}} \, [\mathrm{W/m^2}], \tag{4.1}$$

where A_d is the active area of the photodiode, R is the diode response and τ_f is the transmittance of the optical filter.

The irradiance depends on the distance between the light source (plasma) and the photodiode, because of the inverse-square law of emission and change of the line of sight volume.

Therefore, it is useful to determine the volumetric emission power, which is the characteristic property of the plasma, in the line of sight plasma volume. The average volumetric emission power can be determined from the measured irradiance if the geometric transmission probability of the photons to the photodiode is known. Due to finite plasma volume the transmission probability varies inside the line of sight volume. It can be determined most accurately with a Monte-Carlo simulation. An analytical expression can be used in the case of a simple geometry where diameters of the photodiode and the light emission aperture are small in comparison to the distance between the photodiode and the plasma source. Such expression is derived in publication [PII]. The volumetric radiant emission power for isotropic and homogeneous plasma in the line of sight volume can be calculated from the measured signal as

$$\frac{d\Phi_\mathrm{e}}{dV} = \frac{4\pi(D+\frac{L}{2})^2}{A_\mathrm{d} A_\mathrm{e} L(1+\frac{L}{D}+\frac{1}{3}\frac{L^2}{D^2})} \frac{i}{R\tau_\mathrm{f}}, \, [\mathrm{W/m^3}], \tag{4.2}$$

where D is the distance between the photodiode and the light emission aperture (referred as extraction aperture in the case of ion sources), A_d is the area of the photodiode, A_e is the area of the extraction aperture, L is the length of the plasma volume, i is the measured photodiode current, R [A/W] is the diode response and τ_f is the transmittance of the optical filter.

The assumption of isotropic and homogeneous plasma is typically well justified for the line of sight volume in the middle of the plasma chamber. Scaling the results to cover the entire plasma chamber is somewhat troublesome. The volumetric emission depends on the density of hot electrons (see sections 2.4.1 and 2.3), which is not typically uniform in magnetized plasmas. The minimum total

VUV-emission power was determined in publications [PII] and [PIV] by determining a justified minimum volume for an isotropic and homogeneous plasma. It was concluded that the total VUV-emission power is in the range of 50–100% of the emission calculated by scaling the line of sight emission isotropically and homogeneously to the entire plasma chamber.

A complete error analysis for the measurements is presented in publication [PII]. The relative uncertainty of the emission band measurements is $\pm$13%, which is mostly affected by the uncertainties of the diode response ($\pm$10%) and transmittances ($\pm$8%). The accuracy of the total VUV-emission determined from the signal difference meusured without and with UV-FS/BK7 window is $\pm$20–25%. The uncertainty is higher than in the case of emission band measurements due to small signal difference without and with UV-FS/BK7 window. Thus, the uncertainty of the visible light trasmittance of UV-FS/BK7 windows has a significant contribution to the accuracy.

Information about the reflectance of VUV light for typical plasma chamber materials is challenging to find from the literature. The reflectance of metals in the VUV range is typically <50% (see e.g. Refs. [95–97]). Based on this information it can be estimated that the reflection from the unpolished back plate of the plasma chamber induces a background of few percent or less ($\ll$10%) to the measured signal. This is not taken into account in the following data analysis.

The VUV-irradiance was measured from a filament driven multicusp arc discharge (LIISA) and a 2.45 GHz microwave discharge presented in the following sections.

4.1 LIISA

The filament driven arc discharge negative ion source LIISA (Light Ion–Ion Source Apparatus) is presented in Fig. 13. LIISA is used as an H^- injector for the JYFL K-130 cyclotron [98]. It consists of a decapole (10-pole) multicusp plasma chamber, back plate housing two tantalum filaments, biased plasma electrode and extraction system. The diameter and the length of the plasma chamber are 9 cm and 31 cm, respectively. The plasma chamber is made of copper, but it is coated with tantalum due to the evaporation of the filament. The strength of the cusp field is 300-350 mT on the wall of the plasma chamber. The maximum strength of the magnetic dipole filter field is 30-35 mT on the source axis. More detailed description of the ion source can be found from Refs. [PIV, 98]. LIISA is similar to the TRIUMF type multicusp arc discharge source studied in Refs. [99, 100].

Typical operational parameters of LIISA are 500–1000 W of arc discharge power (by using arc voltage of 35–70 V) and 0.2-0.8 Pa pressure. The ion source can provide an H^--beam of 1.4 mA extracted through 11 mm aperture with 1 kW discharge power. The maximum beam (> 1mA, 1 kW) can be achieved with the co-extracted electron / H^- ratio varying from 16 (0.2 Pa) to less than 2 (>0.5 Pa).

The VUV-irradiance meter was probing the plasma along an axial line of

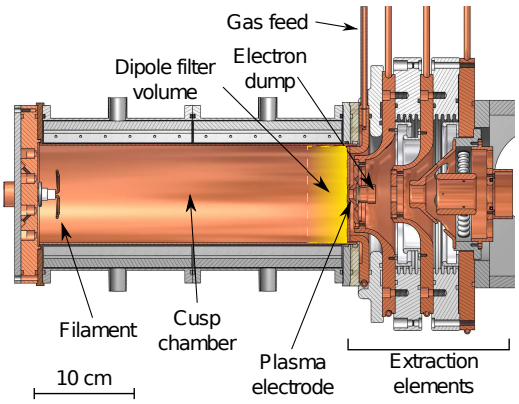

FIGURE 13 A schematic view of the filament driven arc discharge, LIISA.

sight through the extraction aperture from a distance of about 1.5 m. The meter was connected to the beam line, where the pressure was approximately 1×10^{-6} mbar during the measurements. The beam line Faraday cup was used as a shutter between spectrum scans to mitigate the effect of VUV-radiation induced defects of the optical elements.

The source is extremely reliable and the results are well reproducible in comparison to the microwave discharge. For example, the H^-, bias and co-extracted electron currents vary only a few percent when identical parameters (pressure, arc discharge power and plasma electrode voltage) are applied during consecutive runs of the JYFL K-130 cyclotron.

4.2 2.45 GHz microwave ion source

The microwave ion source used in this study (publication [PII]) is presented schematically in Fig. 14. The ion source consists of a microwave coupling system, a cylindrical aluminium plasma chamber surrounded by a single solenoid coil, and an extraction system for positive ions. Microwaves are coupled to the plasma chamber through a rectangular waveguide system, which consists of a 2.45 GHz magnetron, circulator, three stub tuners for impedance matching and a ridged waveguide section. Similar coupling system is frequently used in microwave ion sources (see e.g. Refs. [74,101] and references therein). The vacuum of the plasma chamber is sealed from the waveguide (under atmospheric pressure) by a quartz window embedded into the back plate of plasma chamber. The quartz window is covered by a boron nitride (BN) disc. The diameter and the length of the cylindrical aluminium plasma chamber are 9.5 cm and 10 cm respectively. The ion source is typically operated with 300–1200 W of microwave power in 0.05–10 Pa[1] pressure range. The forward and reflected powers were measured from the magnetron and a power load at the circulator.

[1] Pressure readings in this study were measured with a Pirani gauge including up to a factor 2 uncertainty [102].

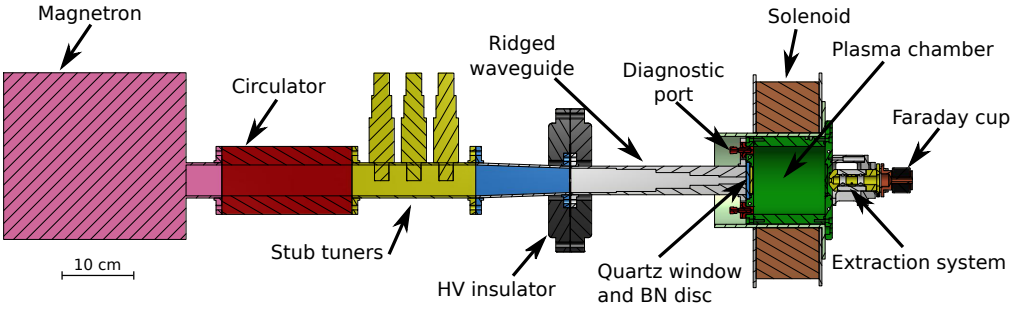

FIGURE 14 A schematic view of the 2.45 GHz microwave ion source. Figure is from Ref. [PII].

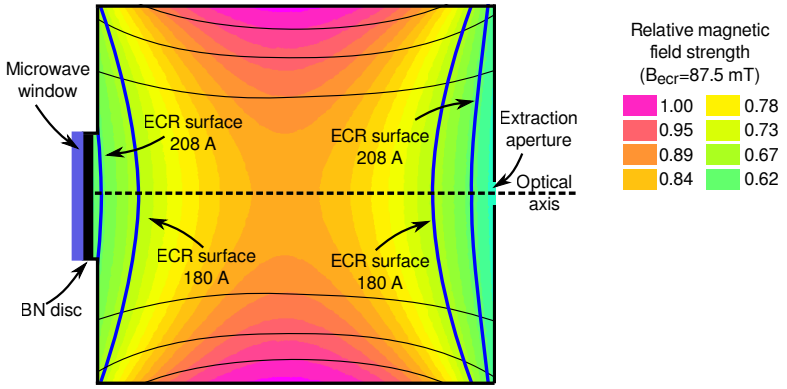

FIGURE 15 Magnetic field topology and ECR surfaces corresponding coil currents of 180 A and 208 A. Data is from publication [PII].

Microwave discharges are typically heated with electron cyclotron resonance (ECR) heating [13]. However, it is possible to sustain the discharge without fullfilling the ECR condition in the plasma chamber [73]. The best performance is typically achieved, when the resonance magnetic field exists close to the microwave window (Fig. 15).

The irradiance meter was located 58.5 cm from a 6 mm diameter extraction aperture. It was necessary to use a magnetic filter in the extraction aperture to suppress an observed plasma jet pluming out of the chamber. Without the filter the plasma jet damaged optical elements and the VUV-emission of the jet caused a significant background signal affecting the measurements. The magnetic filter caused only a weak stray field in the plasma chamber. The plasma source and the irradiance meter were separated with a gate valve and they were pumped separately with turbomolecular pumps. This allowed connecting the irradiance meter to the VUV-spectrometer without venting the plasma source. The gate valve was also used as a shutter in between the VUV-measurements.

The VUV-emission was measured as a function of injected microwave power, neutral gas pressure and magnetic field strength. The most challenging aspect of the multi-dimensional parameter scan was the fact that the source performance depends on the optimization procedure. The performance is sensitive

to impedance matching with the stub tuners, which partially explains the variation of the reflected microwave power as a function of the given source parameters. An unknown fraction of the microwave power was also absorbed by the waveguide system. The significance of the absorption depends on the impedance matching, assembly of the waveguide system and plasma parameters. Thus, the most reliable method to perform systematic studies was to minimize the reflected power by adjusting the stub tuner positions under specific source parameters and use the corresponding tuner settings in all following measurements. The source parameters for the optimization were 600 W microwave power and 0.6 Pa neutral gas pressure at optimum magnetic field (208 A coil current). Such optimization provided good source performance for varying coil current at <700 W microwave power. The measurements were performed after manual cleaning of the plasma chamber followed by several hours (hydrogen) plasma cleaning to minimize the level of residual gases.

5 VUV-DIAGNOSTICS OF ELECTRON IMPACT PROCESSES

Diagnostics of electron impact processes is challenging. Typically different reaction rates are estimated by calculating them directly from equation 2.11 by using measured plasma parameters. This method is very sensitive to uncertainty of plasma parameters, especially the EEDF. Thus, simulation codes have been widely used for studies of plasma processes, but there are concerns about uncertainties and accuracies related to simulations (see e.g. reviews [47, 49, 50]).

Photon emission is rarely applied for diagnostics of plasma processes. It is not discussed in review papers (see e.g. Refs. [36, 51, 103]). The limited number of studies found in the literature are based on diagnostics of molecular processes by using atomic emission. However, using the atomic emission for this purpose is challenging due to multiple excitation channels of the atoms (see section 2.5). For example, Sawada and Fujimoto [104] have developed methods for determining ionization and dissociation rate coefficients of hydrogen molecules based on optical emission spectroscopy of hydrogen atoms in visible light range. Graham has estimated the production rate of ground state hydrogen molecules at high vibrational levels based on (absolute) Lyman-alpha emission and comparison of the rate coefficients of molecular (singlet) and atomic excitations [105]. Lavrov et al. have demonstrated that molecular continuum emission could be used as a probe for dissociation rate in molecular hydrogen plasmas [106]. However, only excitations to $a^3\Sigma_g^+$ and $b^3\Sigma_u^+$ states were taken into account and the total calculated emission was based on an extrapolation of spectral measurement data in the range of 225-450 nm.

Diagnostics of electron impact plasma processes based on the VUV emission of hydrogen plasmas has been developed in this study. The complete description of the diagnostics is presented in publication [PIII]. A brief summary is presented in this chapter. The study focuses on diagnostics of molecular electron impact processes based on the emission by hydrogen molecules (instead of atoms) due to the uncertainty related to the origin of Lyman-alpha emission in molecular hydrogen plasmas. However, the described methods could be applied for the diagnostics of any elemental species, including the hydrogen atom, if the origin

of excitations can be understood.

The main principle of the method is the comparison of probabilities between a certain process (object of the diagnostics) to specific photon emission. For electron impact processes in the corona equilibrium this means comparing the electron impact rate of a certain process to the electron impact excitation rate to specific electronic state. In other words, if the volumetric rate of a specific process (R_1) can be determined e.g. by measuring the volumetric emission rate of a specific band of VUV-light, the volumetric rate of another process (R_2) can be estimated from

$$R_2 = \frac{n_n n_e \alpha_2(T_{vib})}{n_n n_e \alpha_1(T_{vib})} R_1, \tag{5.1}$$

where n_n is the neutral density, n_e is the electron density and $\alpha(T_{vib})$ is the vibrationally weighted rate coefficient (see Eq. 2.12). If the same neutral species (n_n) is involved in both processes, the electron and neutral densities cancel out. Thus, the volumetric rate R_2 can be obtained by multiplying the measured volumetric rate R_1 with the corresponding ratio of rate coefficients, i.e.

$$R_2 = \frac{\alpha_2(T_{vib})}{\alpha_1(T_{vib})} R_1 = K_{2,1}(T_{vib}) R_1, \tag{5.2}$$

where $K_{2,1}$ is the rate coefficient ratio of process to photon emission (excitation).

If the functional shapes of the cross sections of the processes R_1 and R_2 are similar, the coefficient $K_{2,1}$ is typically significantly less sensitive to variation of the EEDF than R_1 or R_2 themselves. This is because $K_{2,1}$ is only sensitive to variation of the EEDF in the energy range, where the ratio of the cross sections varies significantly and the magnitudes of the cross sections are large. This sensitive range is typically narrow and is found close to the threshold energies of the processes. Furthermore, when R_1 and R_2 are similar types of excitations, effects caused by varying vibrational temperature are reduced due to similar vibrational dependence.

The Lyman-band ($B^1\Sigma_u^+ \rightarrow X^1\Sigma_g^+$) and molecular continuum ($a^3\Sigma_g^+ \rightarrow b^3\Sigma_u^+$) emissions are the most suitable transitions for the purpose of plasma diagnostics as explained in section 2.5. Lyman-band and molecular continuum emissions yield information, which is related to singlet or triplet excitations, respectively, as discussed in section 2.3. The Lyman-band emission is proportional to vibrational excitation to high vibrational levels and molecule dissociation via vibrational continuum. Because, the functional shapes of ionization and singlet excitation cross sections are similar, the Lyman-band emission is also proportional to ionization rate. Correspondingly, the molecular continuum emission is proportional to molecule dissociation via triplet states and production of metastable $c^3\Pi_u$ states. The $K_{2,1}$ coefficients for these processes are plotted in publication [PIII] by using Maxwellian and uniform EEDFs.

Complete error analysis of the diagnostics is presented in publication [PIII]. It is concluded that the uncertainty of the absolute values of processes related to singlet excitations (excitation to ν>5, dissociation and ionization) is <32%. The

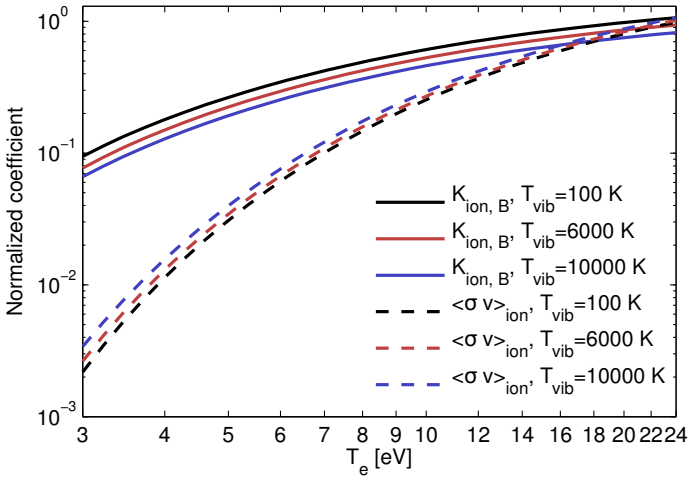

FIGURE 16 Normalized ionization rate coefficient $\langle \sigma v \rangle_{ion}$ and ratio of rate coefficients ($K_{ion,B}$) as a function of electron temperature in different vibrational temperatures. Figure is from Ref. [PIII].

most significant sources of uncertainty are the measurement method (see publication [PII]) and determination of $K_{2,1}$ with minimum knowledge about the EEDF. The uncertainty related to triplet processes is larger due to the metastable $c^3\Pi_u$ state. The $c^3\Pi_u$ state can contribute to molecular continuum emission due to de-excitation or collisional quenching. This causes up to factor of two uncertainty to diagnostics related to triplet states. The uncertainty can be reduced by estimating the role of different de-excitation processes in individual plasma sources as explained in publication [PIII]. It is noteworthy that there are significant uncertainties related to cross sections [25, 40], which are not included to this analysis. The uncertainty caused by the cross section data is challenging to analyze, because the method is only sensitive to uncertainty of the cross section ratio of the studied processes.

The EEDF, the vibrational distribution and the density of metastable molecules are often characteristic properties of the plasma source. Thus, it is possible to measure the relative changes of volumetric reaction rates with significantly improved accuracy in comparison to absolute values. Relative changes are often the most important information required for practical development of plasma sources.

The accuracy of the described diagnostics can be compared to the accuracy of typical rate coefficient calculations by comparing equations 2.11 and 5.2. It can be estimated that the accuracies of plasma and neutral densities in Eq. 2.11 correspond to the accuracy of the volumetric photon emission rate[1] in Eq. 5.2. Thus, the largest difference between the accuracies of the methods is caused by the uncertainty of the EEDF and VDF affecting $\langle v\sigma \rangle$ or $K_{2,1}$. This is demonstrated in Fig. 16, where coefficients ($K_{ion,B}$ and $\langle \sigma v \rangle_{ion}$) are compared in the case of ionization rate and Maxwellian EEDF. Coefficient $K_{ion,B}$ is most sensitive to the EEDF

[1] This overestimates the accuracy of Eq. 2.11, because there are often large uncertainties also in electron and neutral densities.

TABLE 1 Ratios of rate coefficients $K_{2,1}$ for LIISA and 2.45 GHz microwave discharge. The rate coefficients of the reactions are compared to total excitation rate coefficient to $B^1\Sigma_u^+$ state (emitting Lyman-band) or $a^3\Sigma_g^+$ state (emitting molecular continuum) as referred in the table.

	Discharge	
	LIISA	2.45 GHz
Lyman-band		
Molecule ionization	0.9–2.0	0.1–1.3
Excitation ($B^1\Sigma_u^+$, $C^1\Pi_u$)	1.7–1.9	1.4–1.8
Excitation ($\nu \geq 5$) ($B^1\Sigma_u^+$, $C^1\Pi_u$)	1.0–1.1	0.8–1.1
Dissociation ($B^1\Sigma_u^+$, $C^1\Pi_u$)	1.7–1.9	0.2–0.3
Molecular continuum		
Dissociation (via $b^3\Sigma_u^+$)	2.1–4.7	2.2–8.5
Excitation $c^3\Pi_u$ state, max	0.6–1.3	0.6–1.8

and VDF because there are significant differences in threshold energies and vibrational dependencies between the rate coefficients of ionization and excitation to $B^1\Sigma_u^+$ state. However, the coefficient $K_{ion,B}$ varies only an order of magnitude while $\langle \sigma v \rangle_{ion}$ varies almost three orders of magnitude in the same electron temperature range.

Insensitivity of $K_{2,1}$ to the EEDF and VDF allows estimating volumetric rates without accurate knowledge about plasma parameters. For example, coefficients $K_{2,1}$ of different processes are presented for LIISA and the microwave discharge in table 1 by using the largest possible variation of the EEDF and vibrational temperature. The variations correspond to EEDFs with E_{max}=35–70 eV (uniform) in the case of LIISA and T_e=3–23 eV (Maxwellian) in the case of the microwave discharge and vibrational temperature of 100–10000 K. These variations of the EEDFs and VDFs correspond to typical ranges found from low temperature plasma sources (see e.g. Refs. [13, 63, 107]). Thus, it can be argued that the corresponding accuracy (order of magnitude in case of ionization, less than a factor two in the case of singlet excitation and less than a factor three in the case of triplet excitations) can be achieved without making further assumptions about the plasma other than the corona equilibrium.

The presented diagnostics could be developed further. Similar information about electron impact processes could be obtained with visible or infrared spectroscopy if there are suitable singlet and triplet transitions between higher electronic states of the hydrogen molecule. Moreover, the ratio of singlet to triplet emission yields information about the average energy of the hot electrons. Applying this information could reduce the EEDF dependence of the diagnostics.

6 RESULTS

The methods discussed in the previous chapters were applied for diagnostics of hydrogen plasmas of a filament driven arc H^- ion source, LIISA (see detais on section 4.1) and a microwave discharge proton source (see detais on section 4.2). The measured VUV-emissions and analysis of reaction rates are presented in this chapter. The data were originally presented in publications [PII], [PIII] and [PIV].

The behaviour of the VUV-emission as a function of plasma heating power and neutral gas pressure differ significantly between LIISA and the microwave discharge. In LIISA the intensities of Lyman-alpha, Lyman-band and Werner band emission are linearly proportional to the discharge power, while molecular continuum emission is proportional to the discharge current (Fig. 17). In the microwave discharge only Lyman-alpha is linearly proportional to discharge power, while Lyman-band and molecular continuum are insensitive to power variation (Fig. 18). The VUV-emission in LIISA is insensitive to the pressure variation in the (studied) range of 0.2–1 Pa (Fig. 4 in [PIV]). In the microwave discharge the pressure dependency varies between the emission bands (Fig. 6 in [PII]). The Lyman-alpha emission decreases and Lyman-band emission increases, when the neutral gas pressure exceeds 1 Pa. Below 1 Pa neutral gas pressure the Lyman-alpha and Lyman-band are insensitive to changes of the pressure. The molecular continuum emission at optimum coil current (magnetic field) is proportional to neutral gas pressure in the entire pressure range of 0.4–1.6 Pa.

The following comparison of plasma process rates in the given discharges is made at fixed operating parameters of the plasma sources. The discharge power of 1.0 kW can be considered as a nominal value for both discharges. Neutral gas pressures of 0.6 Pa and 0.4 Pa in the microwave discharge and LIISA, respectively, are optimum values in terms of ion beam production. The magnetic field of the microwave discharge is optimized i.e. the resonance surface is found near the microwave window (see Fig. 15).

The volumetric emissions of Lyman-alpha, Lyman-band and molecular continuum in the line of sight volume of LIISA and the microwave discharge are presented in Table 2. The volumetric reaction rates presented in Table 3 were calculated by using the method presented in chapter 5 and coefficients presented in

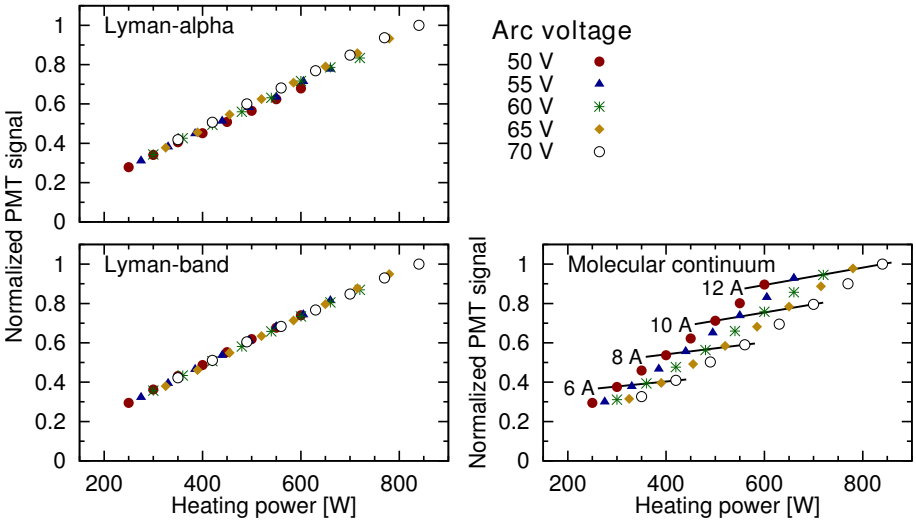

FIGURE 17 LIISA VUV-emission within specific wavelength ranges as a function of discharge power at 0.35 Pa pressure. Data is from Ref. [PIV].

Table 1. In both discharges the order of magnitude of volumetric ionization and excitation rate is 10^{16} $1/\mathrm{cm}^3\mathrm{s}$ at the discharge power of 1 kW. However, the values obtained with LIISA are several times higher. The most significant difference in the electron impact rates between these plasma sources is found in molecule dissociation. Molecule dissociation occurs dominantly via triplet excitations in the microwave discharge, while singlet and triplet channels are comparable in LIISA.

By scaling the reaction rates of the line of sight volume to cover the entire plasma chamber it can be found that in LIISA at least 15–30% of the discharge power is dissipated via photon emission while the corresponding percentage is less than 8% in the microwave discharge. These numbers are consistent with the theory presented in publication [PI] (chapter 3) implying that the heating efficiency of LIISA is close to the theoretical maximum and the heating efficiency of the microwave discharge is rather poor. In both plasma sources each injected molecule undergoes several inelastic collisions including ionizations, excitations and dissociations. The upper limit of metastable states ($2S$ atoms and $c^3\Pi_u$) was estimated from the production rates in publications [PII] and [PIII]. In LIISA it is 0.4% of neutral gas density while in microwave discharge it is 0.5% of neutral gas density.

The ratio of Lyman-band to molecular continuum emission yields information on the average energy of hot electrons. This is because triplet excitation cross sections are peaked at lower electron energies than singlet excitation cross sections (see Fig. 8). The given ratio is approximately four times higher in LIISA than in the microwave discharge implying higher fraction of ionization and $H_2(\nu{>}5)$ production with respect to dissociation via triplet excitation. On the other hand, the total photon emission power, which yields information on the efficiency of plasma heating power dissipation (see Chapter 3), is significantly higher in LIISA than in the microwave discharge [PII–PIV]. Altogether this implies that the

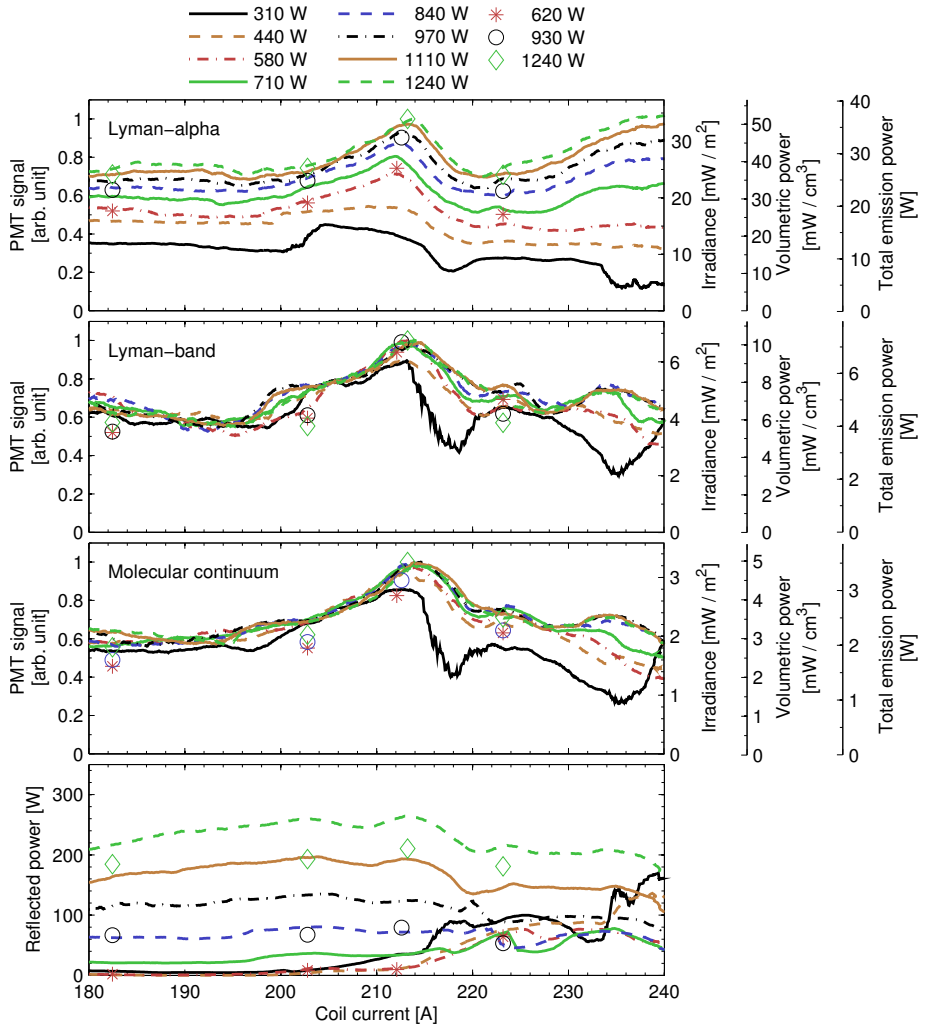

FIGURE 18 Microwave discharge VUV-emission within specific wavelength ranges from the microwave discharge as a function of injected microwave power at 0.6 Pa pressure. Figure is from Ref. [PII].

TABLE 2 Volumetric emission rates of different transitions in the line of sight volume of LIISA and the microwave discharge.The values for LIISA are calculated from the data presented in publication [PIV] by using the correction coefficients presented in publication [PII]. The values for the microwave discharge are from publication [PII].

	Discharge		
	LIISA	2.45 GHz	
Atom			
Lyman-alpha ($2P \rightarrow 1S$)	$\ll 1$	1.0–1.5	$\times 10^{16}$ 1/cm^{3}s
Molecule			
Lyman-band ($B^1\Sigma_u^+ \rightarrow X^1\Sigma_g^+$)	4.5–5.1	1.3–1.6	$\times 10^{16}$ 1/cm^{3}s
Werner-band ($C^1\Pi_u \rightarrow X^1\Sigma_g^+$)	2.25–4.1	0.7–1.0	$\times 10^{16}$ 1/cm^{3}s
Molecular continuum ($a^3\Sigma_g^+ \rightarrow b^3\Sigma_u^+$)	1.3	1.3–1.4	$\times 10^{16}$ 1/cm^{3}s

heating power is not only dissipated more efficiently in LIISA but also the EEDF is more suitable for volume production of H^- ions due to higher fraction of ionization and $H_2(\nu{>}5)$ production rates.

The ratio of Lyman-alpha emission to Lyman-band emission implies that the plasma atomic fraction is several times higher in the microwave driven plasma, which is expected because microwave discharges are efficient proton sources [74]. However, the differences in atom and proton fraction between the two plasma sources can not be explained only by the difference in the total dissociation rate.

There are only a few earlier experiments to which the results presented in this section can be compared. The comparison is complicated by the fact that the experiments have been performed with plasma sources that are based on different mechanical solutions in comparison to this study. The production rate of high vibrational levels in a filament driven arc discharge was estimated earlier by Graham [105] and density of metastable $c^3\Pi_u$ states by Bonnie et al [38]. The discharge used by Graham does not include multicusp confinement and, therefore, the confinement of the energetic electrons emitted by the hot cathode was weak in comparision to LIISA. Thus, it is not surprising that the results obtained by Graham is approximately an order of magnitude lower than those presented here. The discharge used by Bonnie et al is similar to LIISA. However, their result of the density of metastable $c^3\Pi_u^-$ states is approximately two orders of magnitude lower than the estimated upper limit in this study. The difference is probably caused by uncertainties related to the estimate presented in this study i.e. a) the applied cross section is the total cross section to $c^3\Pi_u$ states, b) the contribution of $c^3\Pi_u$ state to the molecular continuum emission c) the estimated maximum effective lifetime of the $c^3\Pi_u^-$ state and d) the assumption of homogeneous and isotropic plasma emission profile. Thus, the estimated maximum $c^3\Pi_u^-$ density presented here is consistent with the measured value given in Ref. [38]. Absolute

TABLE 3 Volumetric rates of different plasma processes in the line of sight volume of LIISA and the microwave discharge. The orginal data is presented in publications [PII] and [PIII].

	Discharge		
	LIISA	2.45 GHz	
Lyman-band			
Molecule ionization	7–15	0.14–2.1	$\times 10^{16}$ 1/cm^{3}s
Excitation ($B^1\Sigma_u^+$, $C^1\Pi_u$)	12–14	1.8–2.8	$\times 10^{16}$ 1/cm^{3}s
Excitation ($\nu \geq 5$) ($B^1\Sigma_u^+$, $C^1\Pi_u$)	7.0–7.8	1.1–1.7	$\times 10^{16}$ 1/cm^{3}s
Dissociation ($B^1\Sigma_u^+$, $C^1\Pi_u$)	1.8–2.0	0.3–0.4	$\times 10^{16}$ 1/cm^{3}s
Molecular continuum			
Dissociation (via $b^3\Sigma_u^+$)	2.5–5.8	2.2–8.5	$\times 10^{16}$ 1/cm^{3}s
Excitation $c^3\Pi_u$ state, max	0.7–1.5	0.6–1.8	$\times 10^{16}$ 1/cm^{3}s

values of molecular continuum emission have been measured earlier from microwave discharges by Fantz et al [65]. They observed volumetric emission rates on the order of 10^{15}–10^{16} 1/cm^{3}s, which is consistent with this study.

The development of ion sources has similarities to evolution in biology. The ion beam intensity and operational reliability are the driving forces in the evolution of ion sources, while in biology it is success of the population. It is well known that microwave and filament driven multicusp arc discharges are on the top of their own evolutionary branches (H^+ and H^- volume production) at the moment[1]. Due to complexity of plasma physics, plasma processes and diagnostics, the progress in ion source performance is more or less achieved through trial and error (i.e. Edisonian approach [12]). Thus, it is not always clear if the current situation is close to a global or a local maximum of the performance. The methods developed in this study allow discussing, why the microwave and filament driven multicusp arc discharges are in their current stages.

The confinement of the electrons emitted by the filament is good in the multicusp arc discharge [13]. As a results the EEDF consists of the cold Maxwellian population which does not excit or ionize neutral gas and the hot population. The hot population is uniformly distributed up to the value corresponding to the cathode potential and is responsible for ionization and electronic excitation of the neutral gas. Thus, the plasma heating power is dissipated efficiently in inelastic collisions and the relative importance of plasma processes can be regulated by adjusting the arc voltage (e.g. ratio of triplet vs. singlet excitations depend on the maximum energy of the uniform hot electron population) or current. Ionization and production of high vibrational levels dominate inelastic collisions at high arc

[1] The highest performance H^- ion sources [67] utilize RF-heating instead of filament arc discharge. This is because of usage of Caesium and longer maintenance periods.

voltages while molecule dissociation and light emission increases at lower voltages (see chapter 3)

The microwave discharge could be expected to perform similarly to the arc discharge at the high arc voltage. This is because ECR-process heats electrons efficiently to high energies [108]. However, in reality, the observed relative importance of triplet and singlet excitations corresponds to low arc voltage in the arc discharge and the total photon emission power is significantly lower in the microwave discharge. This implies that electrons with energies exceeding the plasma potential are not confined by the solenoid magnetic field. The mean free path between inelastic collisions with neutrals is several times longer than the dimensions of the plasma chamber (on the order of 1 m compared to 0.1 m). Although the ECR heating increases the path length of the electrons, the probability of the hot electrons to escape in the direction of the magnetic field without dissipating their energy in inelastic collisions is high. In contrast, the multicusp field in LIISA confines electrons in all directions. Therefore, in the microwave discharge the average energy and total VUV emission are lower than could be expected taking into account the plasma heating method.

Differences between the arc discharge and the microwave discharge can not be explained solely by plasma processes, but also plasma-wall interactions must play a significant role. The total dissociation rate in both discharges is similar, but the proton fraction (and Lyman-alpha fraction of VUV-emission) is significantly higher in the microwave discharge. Boron-nitride (BN) discs have been used in microwave discharges to increase the proton fraction [109]. As explained in section 2.3.1 there is a significant difference in surface association coefficients between metals and insulators. In LIISA constantly replenished metal surface is efficient for atom association. In contrast, association probability on the boron-nitride or oxidized metal surfaces of the microwave discharge ion source can be several orders of magnitude less, which alone could explain the difference in the observed proton fraction.

Altogether this implies that plasma heating is well-optimized for the H^- volume production in the filament driven arc discharge. It might be possible to improve the H^- production by optimizing surface materials and magnetic filters fields. On the other hand, it seems that the microwave discharge is an optimal proton source due to surface properties of the plasma chamber. However, it is far being optimized for the plasma heating efficiency.

Some conclusions can be made, how LIISA could be made an efficient proton source and the microwave discharge an efficient H- source. These conclusion serve as predictions for the changes of plasma properties caused by mechanical modifications.

Probably the most efficient way to affect the proton fraction in the filament driven multicusp arc discharge is to change the plasma chamber material to an insulator. This would also require the filaments to be replaced by thermionic electron emitters which do not suffer from metal evaporation. Furthermore, using lower neutral gas pressure and arc voltage (e.g. <50 V) could enhance the proton fraction due to increased dissociation rate.

Using the microwave discharge as an efficient driver for a magnetically filtered tandem source would require that the entire plasma chamber (both walls and the microwave window) is covered with a material having a high association probability. Improving the confinement of the hot electrons could increase the ionization and production of high vibrational levels when the electron energy is dissipated more efficiently (at high energies). This could also enhance energy efficiency of the plasma source. However, an efficiency matching that of the filament driven multicusp arc discharge might not be possible to achieve with the microwave discharges. This is because ECR heating requires the presence of magnetic field. The confinement of the hot electrons is proportional to the mirror ratio, i.e. the ratio between the maximum magnetic field strength and magnetic field strength in the spatial location where the plasma heating occurs (see Section 2.4.1). Thus, the magnetic confinement is always less efficient in the ECR -heated device than in the filament driven multicusp arc discharge where the electron emission occurs at a location with virtually negligible[2] magnetic field strength.

[2] There is a significant magnetic field on the surface of the filament induced by the filament current. However, this magnetic field is weak in comparison to the multicusp magnetic field on the poles. Furthermore, the electron movements are randomized in the negligible magnetic field between the filament and the multicusp poles.

7 DISCUSSION

Vacuum ultraviolet emission of low temperature hydrogen plasmas is rarely measured quantitatively and applied for plasma diagnostic purposes. In this thesis, we have developed a new theory which predicts the VUV-emission from different types of plasma sources, presented a straightforward technique to measure absolute VUV-emission, and developed a robust diagnostics for electron impact processes.

The presented diagnostics can be utilized in development of ion sources. It provides a complete set of diagnostics tools for plasma heating in order to obtain information about processes related to H^+ H_2^+ and H^- ion production, e.g. ionization, dissociation and production of high vibrational levels. The diagnostics were applied to filament arc and microwave discharges, which are the most commonly used plasma sources for the production of H^- and H^+ ions. The measurements provided information about effects of mechanical solutions on the plasma properties. For example, the results show that the filament driven multicusp arc is superior driver for volume production of H^- ions and the energy efficiency of the microwave discharge is poor. The results also underline that all of the differences between plasmas can not be explained by differences in electron impact processes. For example, the high proton fraction in the microwave discharge is probably due to low hydrogen association probability on the surface of the plasma chamber. These results could provide critical information for development of H^- ion sources towards Caesium free operation and more robust plasma heating technique as required by the developments of proton accelerators and neutral beam heating in magnetic confinement fusion research.

Research of plasma physics has been driven towards non-equilibrium plasmas which is the only reasonable way to describe most of the laboratory plasmas. However, theories of plasma physics are based on equilibria leading to development of complex simulation methods. There are concerns about their validation, sensitivity and accuracy [47, 49, 50] and predictive capabilities [12]. Plasma diagnostics and analytical theories, which are weakly sensitive to plasma parameters are rarely found from the literature.

It can be argued that this thesis takes a small step forward providing predic-

tions about light emission and plasma heating power dissipation of non-equilibrium plasmas in general level. Moreover, the developed diagnostics provides new information about the most significant electron impact processes requiring minimum information about plasma parameters. The diagnostics can be used for benchmarking of existing simulation codes or developing a new type of simulation as discussed in publication [PIII].

The methods presented in this thesis can be applied for a variety of low temperature plasmas, but only first steps are taken here. Predictions made about the light emission in chapter 3 and about the effects of mechanical modifications in chapter 6 demonstrate the relevance of the methods. However, uncertainties related to cross sections, mathematical formalism of the distributions and more precise validation of the methods requires a lot of further work.

REFERENCES

[1] G. S. Suits and J. Martin. Irving langmuir 1881-1957: A biographical memoir. *National Academy of Sciences Biographical Memoir*, page 214, 1974.

[2] D. Meade. 50 years of fusion research. *Nucl. Fusion*, 50(1):014004, 2010.

[3] R. Durrer. The cosmic microwave background: the history of its experimental investigation and its significance for cosmology. *Classical Quant. Grav.*, 32(12):124007, 2015.

[4] A.J. Meadows and D.T. Haar. *Early Solar Physics: The Commonwealth and International Library: Selected Readings in Physics*. Commonwealth and international library: Selected readings in physics. Elsevier Science, 2013.

[5] M. Bacal and M. Wada. Negative hydrogen ion production mechanisms. *Appl. Phys. Rev.*, 2(2):021305, 2015.

[6] O. Tarvainen, T. Kalvas, J. Komppula, H. Koivisto, E. Geros, J. Stelzer, G. Rouleau, K.F. Johnson, and J. Carmichael. Effect of ion escape velocity and conversion surface material on h- production. *AIP Conf. Proc.*, 1390:113, 2011.

[7] D. Takeuchi et al. Direct observation of negative electron affinity in hydrogen-terminated diamond surfaces. *Appl. Phys. Lett.*, 86(15):152103, 2005.

[8] P. Wurz, R. Schletti, and M.R. Aellig. Hydrogen and oxygen negative ion production by surface ionization using diamond surfaces. *Surf. Sci.*, 373(1):56, 1997.

[9] O. Batishchev and K. Molvig. *Kinetic simulation of high $I(sp)$ plasma thruster*. 36th AIAA//ASME//SAE//ASEE Joint Propulsion Conference and Exhibit, 2000.

[10] A. McPherson, N. Rouze, W. B. Westerveld, and J. S. Risley. Calibration of a VUV spectrometer–detector system using synchrotron radiation. *Appl. Opt.*, 25(2):298, 1986.

[11] C. Dong, S. Morita, M. Goto, and E. Wang. Absolute intensity calibration of flat-field space-resolved extreme ultraviolet spectrometer using radial profiles of visible and extreme ultraviolet bremsstrahlung continuum emitted from high-density plasmas in large helical device. *Rev. Sci. Instrum.*, 82(11):113102, 2011.

[12] *Plasma Science: Advancing Knowledge in the National Interest*. The National Academies Press, 2007.

[13] M.A. Lieberman and A.J. Lichtenberg. *Principles of Plasma Discharges and Materials Processing*. Wiley, 2005.

[14] V. M. Donnelly and A. Kornblit. Plasma etching: Yesterday, today, and tomorrow. *J. Vac. Sci. Technol. A*, 31(5):050825, 2013.

[15] H. B. Profijt, S. E. Potts, M. C. M. van de Sanden, and W. M. M. Kessels. Plasma-assisted atomic layer deposition: Basics, opportunities, and challenges. *J. Vac. Sci. Technol. A*, 29(5):050801, 2011.

[16] S. E. Potts, H. B. Profijt, R. Roelofs, and W. M. M. Kessels. Room-temperature ALD of metal oxide thin films by energy-enhanced ALD. *Chem. Vapor. Depos.*, 19(4-6):125–133, 2013.

[17] C. Graves, S. D. Ebbesen, M. Mogensen, and K. S. Lackner. Sustainable hydrocarbon fuels by recycling CO_2 and H_2O with renewable or nuclear energy. *Renew. Ssust. Energ. Rev.*, 15(1):1, 2011.

[18] J.S. Chang. Recent development of plasma pollution control technology: a critical review. *Sci. Technol. Adv. Mat.*, 2(3–4):571, 2001.

[19] R. Brandenburg, H. Lange, T. von Woedtke, M. Stieber, E. Kindel, J. Ehlbeck, and K.-D. Weltmann. Antimicrobial effects of UV and VUV radiation of nonthermal plasma jets. *IEEE Trans. Plasma Sci.*, 37(6):877, June 2009.

[20] E. Ahedo. Plasmas for space propulsion. *Plasma Phys. Control. Fusion*, 53(12):124037, 2011.

[21] R.E.H. Clark and D. Reiter. *Nucl. Fusion Research: Understanding Plasma-Surface Interactions*. Springer Series in Chemical Physics. Springer, 2006.

[22] T. J. Millar. Astrochemistry. *Plasma Sources Sci. Technol.*, 24(4):043001, 2015.

[23] J.M. Hollas. *Modern Spectroscopy*. Wiley, 2004.

[24] D. Manthey. *Orbital Viewer*, Version 1.04, 2004. (www.orbitals.com/orb/ov.htm).

[25] R. K. Janev, D. Reiter, and U. Samm. *Collision processes in low-temperature hydrogen plasmas*, volume JUEL-4105 of *Berichte des Forschungszentrums Jülich*. Forschungszentrum, Zentralbibliothek, Jülich, 2003.

[26] W. L. Wiese and J. R. Fuhr. Accurate atomic transition probabilities for hydrogen, helium, and lithium. *J. Phys. Chem. Ref. Data*, 38(3):565, 2009.

[27] S.A. Astashkevich and B.P. Lavrov. Lifetimes of the electronic-vibrational-rotational states of hydrogen molecule (review). *Opt. Spectrosc.*, 92(6):818, 2002.

[28] W. L. Fite, R. T. Brackmann, D. G. Hummer, and R. F. Stebbings. Lifetime of the 2*s* state of atomic hydrogen. *Phys. Rev.*, 116:363, 1959.

[29] G.W.F. Drake. *Springer Handbook of Atomic, Molecular, and Optical Physics*. Springer Handbook of Atomic, Molecular, and Optical Physics. Springer, 2006.

[30] U. Fantz and D. Wünderlich. Franck–condon factors, transition probabilities, and radiative lifetimes for hydrogen molecules and their isotopomeres. *Atom. data nucl. data*, 92(6):853, 2006.

[31] M. Cacciatore, M. Capitelli, and G.D. Billing. Vibration-to-translation energy exchanges in H_2 colliding with highly vibrationally excited H_2 molecules. *Chem. Phys. Lett.*, 157(4):305, 1989.

[32] S. Gough, C. Schermann, F. Pichou, M. Landau, I. Cadez, and R. I. Hall. The formation of vibrationally excited hydrogen molecules on carbon surfaces. *Astron. Astrophys.*, 305:687, 1996.

[33] A. S. Muzas, J. I. Juaristi, M. Alducin, R. Díez Muiño, G. J. Kroes, and C. Díaz. Vibrational deexcitation and rotational excitation of H_2 and D_2 scattered from Cu(111): Adiabatic versus non-adiabatic dynamics. *J. Chem. Phys.*, 137(6), 2012.

[34] K. Golibrzuch, N. Bartels, D. J. Auerbach, and Alec M. Wodtke. The dynamics of molecular interactions and chemical reactions at metal surfaces: Testing the foundations of theory. *Annu. Rev. Phys. Chem.*, 66(1):399, 2015. PMID: 25580627.

[35] M. Capitelli, R. Celiberto, F. Esposito, and A. Laricchiuta. Molecular dynamics for state-to-state kinetics of non-equilibrium molecular plasmas: State of art and perspectives. *Plasma Process. Polym.*, 6(5):279, 2009.

[36] J. Boffard, C. Lin, and C. DeJoseph Jr. Application of excitation cross sections to optical plasma diagnostics. *J. Phys. D: Appl. Phys.*, 37(12):R143, 2004.

[37] M. Glass-Maujean. Collisional quenching of H(2S) atoms by molecular hydrogen: Two competitive reactions. *Phys. Rev. Lett.*, 62:144, Jan 1989.

[38] J. H. M. Bonnie, P. J. Eenshuistra, and H. J. Hopman. Rotational temperatures and densities of metastable H_2 in a multicusp ion source. *Phys. Rev. A*, 37:4407, 1988.

[39] H. Tawara, Y. Itikawa, H. Nishimura, and M. Yoshino. Cross sections and related data for electron collisions with hydrogen molecules and molecular ions. *J. Phys. Chem. Ref. Data*, 19(3):617, 1990.

[40] J.-S. Yoon, M.-Y. Song, J.-M. Han, S. H. Hwang, W.-S. Chang, B. Lee, and Y. Itikawa. Cross sections for electron collisions with hydrogen molecules. *J. Phys. Chem. Ref. Data*, 37(2):913, 2008.

[41] R. P. Freis and J. R. Hiskes. Radiative lifetimes for the $2p\pi^3\Pi_u$ state of the hydrogen molecule. *Phys. Rev. A*, 2:573, 1970.

[42] R. Celiberto, M. Capitelli, and A. Laricchiuta. Towards a cross section database of excited atomic and molecular hydrogen. *Phys. Scripta*, 2002(T96):32, 2002.

[43] R. Celiberto, R. K. Janevand A. Laricchiuta, M. Capitelli, J. M. Wadehra, and D. E. Atems. Cross section data for electron-impact inelastic processes of vibrationally excited molecules of hydrogen and its isotopes. *At. Data Nucl. Data Tables*, 77(2):161, 2001.

[44] V. A. Shakhatov and Yu. A. Lebedev. Collisional-radiative model of hydrogen low-temperature plasma: Processes and cross sections of electron-molecule collisions. *High Temperature*, 49(2):257, 2011.

[45] Wikipedia. Navier–stokes existence and smoothness — Wikipedia, the free encyclopedia, 2015. [Online; accessed 4-September-2015].

[46] I.G. Brown. *The Physics and Technology of Ion Sources*. Wiley-Interscience publication. Wiley, 1989.

[47] M. J. Kushner. Hybrid modelling of low temperature plasmas for fundamental investigations and equipment design. *J. Phys. D: Appl. Phys.*, 42(19):194013, 2009.

[48] P. Tian and M. J. Kushner. Controlling VUV photon fluxes in low-pressure inductively coupled plasmas. *Plasma Sources Sci. Technol.*, 24(3):034017, 2015.

[49] H. C. Kim, F. Iza, S. S. Yang, M. Radmilović-Radjenović, and J. K. Lee. Particle and fluid simulations of low-temperature plasma discharges: benchmarks and kinetic effects. *J. Phys. D: Appl. Phys.*, 38(19):R283, 2005.

[50] M. M. Turner. Uncertainty and error in complex plasma chemistry models. *Plasma Sources Sci. Technol.*, 24(3):035027, 2015.

[51] U. Fantz et al. Spectroscopy - a powerful diagnostic tool in source development. *Nucl. Fusion*, 46(6):S297, 2006.

[52] M. Bacal, A. Hatayama, and J. Peters. Volume production negative hydrogen ion sources. *IEEE Trans. Plasma Sci.*, 33(6):1845, 2005.

[53] S. Markelj and I. Čadež. Production of vibrationally excited hydrogen molecules by atom recombination on Cu and W materials. *J. Chem. Phys.*, 134(12):124707, 2011.

[54] O. Gabriel, D. C. Schram, and R. Engeln. Formation and relaxation of rovibrationally excited h_2 molecules due to plasma-surface interaction. *Phys. Rev. E*, 78:016407, 2008.

[55] N. H. Nahler and Alec M. Wodtke. Dynamics of molecule-induced electron emission from surfaces. *Mol. Phys.*, 106(16-18):2227, 2008.

[56] B. Xiao, S. Kado, K. Kobayashi, and S. Tanaka. Numerical simulation of hydrogen molecular dissociation and the effects to H_α profiles in low temperature plasmas. *J. Nuscl. Mater.*, 290-293:793, 2001. 14th Int. Conf. on Plasma-Surface Interactions in Controlled Fusion Devices.

[57] K. Behringer and U. Fantz. Spectroscopic diagnostics of glow discharge plasmas with non-Maxwellian electron energy distributions. *J. Phys. D: Appl. Phys.*, 27(10):2128, 1994.

[58] G. Hagelaar and L. Pitchford. Solving the boltzmann equation to obtain electron transport coefficients and rate coefficients for fluid models. *Plasma Sources Sci. Technol.*, 14(4):722, 2005.

[59] J. Sun, X. Li, C. Sang, W. Jiang, P. Zhang, and D. Wang. Particle-in-cell simulation of hydrogen discharge driven by combined radio frequency and pulse sources. *Phys. Plasmas*, 17(10), 2010.

[60] T. Shibata et al. Analysis of electron temperature distribution by kinetic modeling of electron energy distribution function in JAEA 10 ampere negative ion source. *AIP Conf. Proc.*, 1515(1):177, 2013.

[61] D. Pagano, C. Gorse, and M. Capitelli. Modeling multicusp negative-ion sources. *IEEE Trans. Plasma Sci.*, 35(5):1247, 2007.

[62] J. Bretagne, G. Delouya, C. Gorse, M. Capitelli, and M. Bacal. Electron energy distribution functions in electron-beam-sustained discharges: application to magnetic multicusp hydrogen discharges. *J. Phys. D: Appl. Phys.*, 18(5):811, 1985.

[63] M. Capitelli et al. Vibrational kinetics, electron dynamics and elementary processes in H_2 and D_2 plasmas for negative ion production: modelling aspects. *Nucl. Fusion*, 46(6):S260, 2006.

[64] Y. Golubovskii, S. Gorchakov, and D. Uhrlandt. Transport mechanisms of metastable and resonance atoms in a gas discharge plasma. *Plasma Sources Sci. Technol.*, 22(2):023001, 2013.

[65] U. Fantz, B. Schalk, and K. Behringer. Calculation and interpretation of the continuum radiation of hydrogen molecules. *New J. Phys.*, 2(1):7, 2000.

[66] X. Liu, D E Shemansky, H Abgrall, E Roueff, S M Ahmed, and J M Ajello. Electron impact excitation of H_2: resonance excitation of $B^1\Sigma_u^+(J_j{=}2, v_j{=}0)$ and effective excitation function of $EF^1\Sigma_g^+$. *J Phys. B: At. Mol. Opt*, 36(2):173, 2003.

[67] D.P. Moehs, J. Peters, and Joseph Sherman. Negative hydrogen ion sources for accelerators. *IEEE Trans. Plasma Sci.*, 33(6):1786, Dec 2005.

[68] A. V. Phelps and Z. Lj. Petrovic. Cold-cathode discharges and breakdown in argon: surface and gas phase production of secondary electrons. *Plasma Sources Sci. Technol.*, 8(3):R21, 1999.

[69] T. Lafleur and P. Chabert. Is collisionless heating in capacitively coupled plasmas really collisionless? *Plasma Sources Sci. Technol.*, 24(4):044002, 2015.

[70] I. S. Hong, Y. S. Hwang, and Y. S. Cho. Development of a negative hydrogen ion source for tandem proton accelerator using transformer couled plasma sources. *Rev. Sci. Instrum.*, 73(2):979, 2002.

[71] R. F. Welton, M. P. Stockli, S. N. Murray, Y. Kang, and J. Peters. Initial tests of the spallation neutron source h- ion source with an external antenna. *Rev. Sci. Instrum.*, 77(3):03A508, 2006.

[72] M. P. Stockli, B. Han, S. N. Murray, T. R. Pennisi, M. Santana, and R. F. Welton. Ramping up the spallation neutron source beam power with the H^- source using 0 mg cs/daya). *Rev. Sci. Instrum.*, 81(2):02A729, 2010.

[73] J. Komppula, T. Kalvas, H. Koivisto, J. Laulainen, and O. Tarvainen. An experimental study of waveguide coupled microwave heating with conventional multicusp negative ion sources. *AIP Conf. Proc.*, 1655(1):070004, 2015.

[74] S. Gammino, L. Celona, G. Ciavola, F. Maimone, and D. Mascali. Review on high current 2.45 GHz electron cyclotron resonance sources (invited)a). *Rev. Sci. Instrum.*, 81(2):02B313, 2010.

[75] G. Hellblom and C. Jacquot. Extraction of volume produced H^- ions from a mirror electron cyclotron resonance source. *Nucl Instrum Meth A*, 243(2):255, 1986.

[76] R. Gobin et al. Two approaches for H^- ion production with 2.45 GHz ion sources. *Nucl. Fusion*, 46(6):S281, 2006.

[77] R. Keller, J. Kwan, S. Hahto, M. Regis, and J. Wallig. Plasma and beam production experiments with HYBRIS, a microwave-assisted H^- ion source. *AIP Conf. Proc.*, 925(1):164, 2007.

[78] T. Ichikawa, T. Kasuya, T. Kenmotsu, S. Maeno, T. Nishida, M. Nishiura, H. Yamaoka, and M. Wada. Optimization of magnetic field structure of a compact 14 GHz ecr ion source. *AIP Conf. Proc.*, 1515(1):394, 2013.

[79] S. Béchu, A. Soum-Glaude, A. Bés, A. Lacoste, P. Svarnas, S. Aleiferis, A. A. Ivanov, and M. Bacal. Multi-dipolar microwave plasmas and their application to negative ion production. *Phys. Plasmas*, 20(10):101601, 2013.

[80] D. Sahu, S. Bhattacharjee, M. J. Singh, M. Bandyopadhyay, and A. Chakraborty. Optimization of negative ion current in a compact microwave driven upper hybrid resonance multicusp plasma source. *Rev. Sci. Instrum.*, 83(2), 2012.

[81] S. X. Peng et al. CW/pulsed H^- ion beam generation with PKU Cs-free 2.45 GHz microwave driven ion source. *AIP Conf. Proc.*, 1655(1):070005, 2015.

[82] D. Monahan and M. Turner. On the global model approximation. *Plasma Sources Sci. Technol.*, 18(4):045024, 2009.

[83] B. Meerson. Nonlinear dynamics of radiative condensations in optically thin plasmas. *Rev. Mod. Phys.*, 68:215, Jan 1996.

[84] M. Salvermoser and D. E. Murnick. Efficient, stable, corona discharge 172 nm xenon excimer light source. *J. Appl. Phys.*, 94(6):3722, 2003.

[85] C. S. Sartori, F. J. da Paixão, and M. A. P. Lima. Transitions between excited electronic states of H_2 molecules by electron impact. *Phys. Rev. A*, 58:2857, Oct 1998.

[86] M. Goto, K. Sawada, and T. Fujimoto. Relations between the ionization or recombination flux and the emission radiation for hydrogen and helium in plasma. *Phys. Plasmas*, 9(10), 2002.

[87] J.A. Wesson et al. Disruptions in JET. *Nucl. Fusion*, 29(4):641, 1989.

[88] J. F. Drake. Marfes: Radiative condensation in tokamak edge plasma. *Phys. Fluids*, 30(8):2429, 1987.

[89] J. Yan, A. El-Dakrouri, M. Laroussi, and M. C. Gupta. 121.6 nm radiation source for advanced lithography. *J. Vac. Sci. Technol. B*, 20(6):2574, 2002.

[90] B. Wu and A. Kumar. Extreme ultraviolet lithography: A review. *J. Vac. Sci. Technol. B*, 25(6):1743, 2007.

[91] J. Stephens, A. Fierro, D. Trienekens, J. Dickens, and A. Neuber. Optimizing drive parameters of a nanosecong, pepetitively pulsed microdischarge high power 121.6 nm source. *Plasma Sources Sci. Technol.*, 24(1):015013, 2015.

[92] J.Z. Klose and W.L. Wiese. Branching ratio technique for vacuum UV radiance calibrations: Extensions and a comprehensive data set. *J. Quant. Spectros. Ra.*, 42(5):337, 1989.

[93] D. S. Gray, S. C. Luckhardt, L. Chousal, G. Gunner, A. G. Kellman, and D. G. Whyte. Time resolved radiated power during tokamak disruptions and spectral averaging of AXUV photodiode response in DIII-D. *Rev. Sci. Instrum.*, 75(2):376, 2004.

[94] A. Morozov, T. Heindl, R. Krücken, A. Ulrich, and J. Wieser. Conversion efficiencies of electron beam energy to vacuum ultraviolet light for Ne, Ar, Kr, and Xe excited with continuous electron beams. *J. Appl. Phys.*, 103(10):103301, 2008.

[95] L.R. Canfield, G. Hass, and W.R. Hunter. The optical properties of evaporated gold in the vacuum ultraviolet from 300 Å to 2 000 Å. *J. Phys. France*, 25:124, 1964.

[96] H. P. Hughes and W. Y. Liang. Vacuum ultraviolet reflectivity spectra of the molybdenum and tungsten dichalcogenides. *J. Phys. C: Solid State*, 7(5):1023, 1974.

[97] R. P. Madden, L. R. Canfield, and G. Hass. On the vacuum-ultraviolet reflectance of evaporated aluminum before and during oxidation∗. *J. Opt. Soc. Am.*, 53(5):620, 1963.

[98] T. Kuo, R. Baartman, G. Dutto, S. Hahto, J. Ärje, and E. Liukkonen. A high intensity dc H^- source for low energy injection. *Rev. Sci. Instrum.*, 73(2):986, 2002.

[99] T. Kuo, D. Yuan, K. Jayamanna, M. McDonald, R. Baartman, P. Schmor, and G. Dutto. On the development of a 15 mA direct current H^- multicusp source. *Rev. Sci. Instrum.*, 67(3):1314, 1996.

[100] Y. S. Hwang, G. Cojocaru, D. Yuan, M. McDonald, K. Jayamanna, G. H. Kim, and G. Dutto. Characterization of TRIUMF dc H^- ion sources for enhanced brightness. *Rev. Sci. Instrum.*, 77(3):03A509, 2006.

[101] T. Taylor and J. F. Mouris. An advanced high-current low-emittance dc microwave proton source. *Nucl. Instrum. Meth. A*, 336(1):1, 1993.

[102] Operating manual of Balzers TPR 010 pirani gauge.

[103] M. Capitelli et al. From cold to fusion plasmas: spectroscopy, molecular dynamics and kinetic considerations. *J. Phys. B-At. Mol. Opt.*, 43(14):144025, 2010.

[104] K. Sawada and T. Fujimoto. Effective ionization and dissociation rate coefficients of molecular hydrogen in plasma. *J. Appl. Phys.*, 78(5):2913, 1995.

[105] W. G. Graham. Vacuum ultraviolet emission and H^- production in a low pressure hydrogen plasma. *J. Phys. D: Appl. Phys.*, 17(11):2225, 1984.

[106] B. P. Lavrov, A. S. Melnikov, M. Käning, and J. Röpcke. UV continuum emission and diagnostics of hydrogen-containing nonequilibrium plasmas. *Phys. Rev. E*, 59:3526, 1999.

[107] H. Conrads and M. Schmidt. Plasma generation and plasma sources. *Plasma Sources Sci. Technol.*, 9(4):441, 2000.

[108] R. Geller. *Electron Cyclotron Resonance Ion Sources and ECR Plasmas*. Taylor & Francis, 1996.

[109] O. Waldmann and B. Ludewigt. Measurements of beam current density and proton fraction of a permanent-magnet microwave ion source. *Rev. Sci. Instrum.*, 82(11):113505, 2011.